

Enabling Population-Level Parallelism in Tree-Based Genetic Programming for GPU Acceleration

Zhihong Wu, Lishuang Wang, Kebin Sun, Zhuozhao Li, and Ran Cheng

Abstract—Tree-based Genetic Programming (TGP) is a widely used evolutionary algorithm for tasks such as symbolic regression, classification, and robotic control. Due to the intensive computational demands of running TGP, GPU acceleration is crucial for achieving scalable performance. However, efficient GPU-based execution of TGP remains challenging, primarily due to three core issues: (1) the structural heterogeneity of program individuals, (2) the complexity of integrating multiple levels of parallelism, and (3) the incompatibility between high-performance CUDA execution and flexible Python-based environments. To address these issues, we propose EvoGP, a high-performance framework tailored for GPU acceleration of TGP via population-level parallel execution. First, EvoGP introduces a tensorized representation that encodes variable-sized trees into fixed-shape, memory-aligned arrays, enabling uniform memory access and parallel computation across diverse individuals. Second, EvoGP adopts an adaptive parallelism strategy that dynamically combines intra- and inter-individual parallelism based on dataset size, ensuring high GPU utilization across a broad spectrum of tasks. Third, EvoGP embeds custom CUDA kernels into the PyTorch runtime, achieving seamless integration with Python-based environments such as Gym, MuJoCo, Brax, and Genesis. Experimental results demonstrate that EvoGP achieves a peak throughput exceeding 10^{11} GPops/s. Specifically, this performance represents a speedup of up to $304\times$ over existing GPU-based TGP implementations and $18\times$ over state-of-the-art CPU-based libraries. Furthermore, EvoGP maintains comparable accuracy and exhibits improved scalability across large population sizes. EvoGP is open source and accessible at <https://github.com/EMI-Group/evogp>.

Index Terms—Genetic programming, parallel algorithm, graphics processing unit (GPU), compute unified device architecture (CUDA).

I. INTRODUCTION

GENETIC Programming (GP) [1] is an evolutionary algorithm that autonomously evolves computer programs based on the principles of natural selection and genetic inheritance. In contrast to black-box models such as neural networks, GP produces human-interpretable solutions and allows the structure of the program to evolve dynamically, rather than being fixed in advance. This capability to simultaneously search over both structural and parametric spaces reduces manual design effort and mitigates model bias, making GP a highly

flexible and interpretable machine learning paradigm [2], [3]. Since its inception in the early 1990s [4], GP has undergone extensive development, leading to a variety of variants that differ in their program representations and manipulation strategies. Based on structural representation, GP can be broadly classified into Linear GP [5], [6], Cartesian GP [7], [8], Gene Expression Programming [9], and Grammatical Evolution [10]. Among these, Tree-based Genetic Programming (TGP) has emerged as the most widely adopted variant [11], [12], striking a favorable balance between evolutionary search efficiency and interpretability. In TGP, programs are encoded as hierarchical tree structures, where internal nodes represent operators and leaf nodes denote variables or constants. This tree-based representation facilitates flexible and expressive modeling, and enables efficient evolutionary search via genetic operators such as crossover and mutation. As a result, TGP has been successfully applied to a wide range of tasks, including symbolic regression [13]–[16], classification [17]–[19], complex system design [20]–[23], and robotic control [24]–[26].

While TGP has been successfully applied across a variety of domains, most existing implementations remain constrained to CPU-based execution [27]–[29]. Although CPUs may suffice for small-scale problems, their performance rapidly degrades as data volume and task complexity increase. In modern applications, evaluating individuals often involves processing large datasets or simulating interactions within complex environments, i.e., a procedure that must be repeated for every member of the evolving population. This substantial computational overhead presents a major barrier to algorithmic refinement, particularly in tuning critical hyperparameters. It also severely restricts the adoption of meta-optimization strategies, such as automatic parameter tuning and adaptive operator selection, which have been shown to significantly enhance algorithm performance [30]–[32]. These strategies typically require executing a large number of configurations, which becomes infeasible under high computational cost. Consequently, the excessive evaluation time not only renders TGP impractical for large-scale or complex problems, but also hinders its evolution and adaptability through higher-level optimization mechanisms. This substantially limits the practical utility of TGP in real-world scenarios where scalability, responsiveness, and adaptability are crucial.

To meet the growing computational demands, increasing efforts have been devoted to leveraging modern hardware architectures (e.g., GPUs) which offer massive parallelism and high throughput. Specifically, two intuitive parallelization strategies have emerged to harness GPU capabilities for TGP. The first strategy, known as intra-individual parallelism, involves evalu-

The first three authors contributed equally to this work.

Zhihong Wu, Lishuang Wang, Kebin Sun, and Zhuozhao Li are with the Department of Computer Science and Engineering, Southern University of Science and Technology, Shenzhen 518055, China. E-mails: {zhihong2718, wanglishuang22, sunkebin.cn}@gmail.com, lizz@sustech.edu.cn.

Ran Cheng is with the Department of Data Science and Artificial Intelligence, and the Department of Computing, The Hong Kong Polytechnic University, Hong Kong SAR, China. E-mail: ranchengcn@gmail.com. (*Corresponding author: Ran Cheng*).

ating a single individual across all data points in parallel. This approach is particularly well-suited for tasks such as symbolic regression and classification on large datasets, drawing inspiration from batch processing paradigms in deep learning. Most existing GPU-accelerated TGP implementations adopt this model, as it aligns naturally with the Single Instruction, Multiple Data (SIMD) execution model of GPU hardware [33]–[35]. The second strategy, known as inter-individual parallelism, capitalizes on the inherent parallelism of evolutionary algorithms by simultaneously evaluating multiple candidate solutions. This form of population-level parallelism has been shown to be effective and has become a core component of modern high-performance evolutionary computation. On one hand, it forms the basis of frameworks built on deep learning libraries such as JAX (e.g., EvoJAX [36], evosax [37]) and PyTorch (e.g., EvoTorch [38]). On the other hand, similar strategies have been adopted in distributed general-purpose frameworks such as EvoX [39] and in domain-specific acceleration, including neuroevolution [40] and evolutionary multiobjective optimization [41], [42]. However, despite its adoption in these areas, population-level parallelism remains relatively unexplored in TGP. When applied to TGP, inter-individual parallelism enables concurrent execution of both fitness evaluations and genetic operations (e.g., crossover, mutation, and selection), significantly reducing computational overhead. More importantly, it lays a solid foundation for scaling TGP to much larger populations, thereby enhancing both efficiency and exploratory capacity.

However, efficiently parallelizing TGP at the population level on GPUs remains fundamentally challenging due to several critical technical obstacles. First, the most fundamental difficulty lies in the inherent structural heterogeneity of TGP individuals. Unlike tensor-based models, where computational structures are uniform and well-aligned for parallel execution, TGP individuals can vary significantly in size, topology, and evaluation logic. This structural diversity renders mainstream tensor computation frameworks such as TensorFlow [43] and PyTorch [44] ill-suited for TGP. Even with the fine-grained control provided by low-level frameworks like CUDA, efficient GPU execution requires encoding these variable structures into a regularized and memory-aligned format [45], which is a problem that remains largely unsolved. Second, although data-level parallelism aligns naturally with the SIMD architecture of GPUs and has been effectively exploited in prior work, integrating it with inter-individual (population-level) parallelism introduces substantial system complexity. When both forms of parallelism are considered, the system must coordinate memory layouts, optimize kernel fusion, and manage execution scheduling to prevent resource contention and ensure high throughput. These trade-offs pose significant challenges in maintaining computational efficiency. Third, many practical TGP applications are deployed in Python-based ecosystems such as OpenAI Gym [46], MuJoCo [47], Brax [48], and Genesis [49]. For a GPU-accelerated TGP system to be usable in these contexts, it must provide seamless Python interoperability without sacrificing performance. Achieving this balance between execution speed, development flexibility, and system extensibility constitutes a nontrivial

engineering challenge.

To address the above challenges, we present EvoGP, a high-performance framework tailored for efficient and fully parallel population-level execution of TGP on GPUs. EvoGP tackles the fundamental barriers of structural heterogeneity, multi-dimensional parallelism, and system integration through the following key contributions:

- 1) We propose a tensorized representation for population-level parallelism on GPUs, which transforms structurally diverse TGP individuals into fixed-size, memory-aligned arrays and enables consistent memory access for high-throughput execution. Based on this design, EvoGP is the first framework to achieve GPU acceleration across all evolutionary stages, including initialization, evaluation, and genetic operations.
- 2) We develop an adaptive parallelism strategy for fitness evaluation, which dynamically combines intra-individual and inter-individual execution based on dataset size. This approach allows EvoGP to maintain high GPU utilization and consistently efficient evaluation across tasks with varying input scales.
- 3) We enhance the flexibility and extensibility of EvoGP through high-performance integration with Python environments. By embedding custom CUDA operators into the PyTorch runtime, EvoGP enables seamless deployment in platforms such as Gym, MuJoCo, Brax, and Genesis, while offering rich features and customizable interfaces for research and application development.
- 4) We empirically evaluate the proposed EvoGP. Extensive experiments demonstrate that EvoGP attains a peak throughput exceeding 10^{11} GPop/s, achieves speedups of up to $304\times$ over GPU-based TGP implementations and $18\times$ over the fastest CPU-based libraries, and improves scalability for large population sizes.

The remainder of this paper is structured as follows. Section II introduces the fundamentals of TGP, describes the GPU computing model, and discusses existing TGP implementations. Section III presents our tensorization strategy and adaptive evaluation scheme that enable scalable and efficient GPU-based execution of TGP. Section IV details the implementation of the EvoGP system, including its integration with Python platforms and support for extensibility and multi-output programs. Section V reports the experimental results that validate the effectiveness and efficiency of our approach. Finally, Section VI concludes the paper.

II. BACKGROUND

In this section, we provide an overview of the key background concepts relevant to this work. We begin by briefly reviewing the fundamentals of TGP, followed by an introduction to GPU architecture and the CUDA programming model. We then summarize representative existing TGP implementations, highlighting their capabilities and limitations in the context of parallel execution.

A. Tree-based Genetic Programming

TGP is a core evolutionary algorithm with broad applicability across several domains. In symbolic regression, TGP

is widely used to discover mathematical expressions from data, effectively modeling complex relationships between variables [13]–[16]. For classification tasks, TGP evolves both feature extraction methods and classification rules, facilitating the development of interpretable models [17]–[19]. In complex system design, TGP has been successfully used to automate the creation and optimization of electronic circuits, antennas, and other sophisticated systems [20]–[23]. Furthermore, TGP has shown effectiveness in robotic control by automatically generating robust control strategies for dynamic and uncertain environments [24]–[26].

In TGP, candidate solutions are represented as tree structures that explicitly define the computational flow from input to output. Formally, a TGP tree can be described as

$$T = (V, E, r),$$

where V is the set of nodes, $E \subseteq V \times V$ is the set of edges, and $r \in V$ is the distinguished root node. Every node $v \in V \setminus \{r\}$ has exactly one parent.

A TGP tree represents a function Func that maps an input vector \mathbf{x} to an output y :

$$y = \text{Func}(\mathbf{x}).$$

The computation proceeds in a bottom-up manner: each node v calculates its result $\text{res}[v]$, and the root node's result $\text{res}[r]$ serves as the final output y . Each node in the tree is represented by a tuple $v = (t, \text{val})$, where t is the node type, and val stores the node's value. Nodes in a TGP tree fall into three categories:

Constant Node: This represents a numerical constant. Its computation is:

$$\text{res}[v] = \text{val}.$$

Variable Node: This represents an input variable. Here, val indicates the index of the input vector \mathbf{x} , and its computation is:

$$\text{res}[v] = \mathbf{x}[\text{val}].$$

Function Node: This represents a mathematical or logical function. In this case, val specifies the function type f , and its computation is:

$$\text{res}[v] = f(\text{res}[c_1], \text{res}[c_2], \dots, \text{res}[c_n]),$$

where c_1, c_2, \dots, c_n are the children of the node.

By using this tree-based representation, TGP supports flexible modeling of mathematical expressions and decision processes, which constitute the foundation of Genetic Programming. Fig. 1 shows an example of TGP trees.

TGP iteratively refines a population of trees through a series of genetic operations, including selection, crossover, and mutation, to evolve optimal or near-optimal solutions. Selection is a process that chooses individuals from the population based on their performance, ensuring that better-performing solutions have a higher probability of propagating to subsequent generations. Crossover involves exchanging information between selected parent trees, facilitating genetic diversity and exploration of the solution space. Mutation introduces random modifications by altering nodes or branches

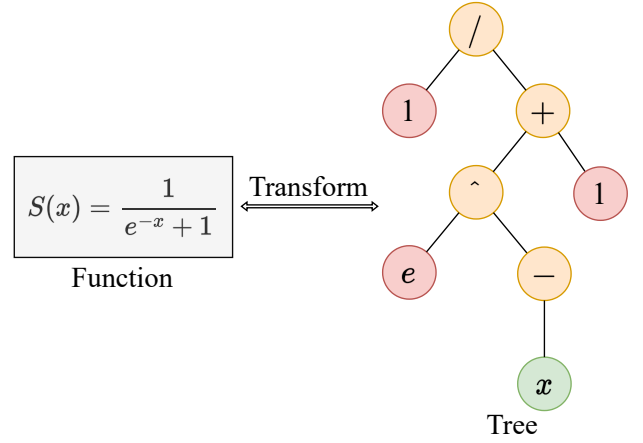


Fig. 1: An example of a tree. In TGP, a computational process is represented as a tree structure. The tree shown in the figure illustrates the sigmoid function. In the figure, the orange nodes represent function nodes, the red nodes represent constant nodes, and the green nodes represent variable nodes.

within an individual tree, thus promoting further diversity and preventing premature convergence [50]. The evolutionary process is described in Algorithm 1.

B. GPU Architecture and CUDA Programming

With the increasing demand for parallel computing, GPUs have evolved into highly efficient accelerators for data-intensive tasks. Modern GPUs consist of thousands of processing cores organized into Streaming Multiprocessors (SMs), enabling massive parallelism. The memory hierarchy includes high-latency global memory, multilevel caches (L1, L2) for faster access, and constant memory optimized for read-only data [51]. However, due to issues such as thread contention, synchronization overhead and fragmentation, dynamic memory management on GPUs exhibits significantly slower perfor-

Algorithm 1 Main Process of TGP

Require: Population size N ; Target fitness f_{target} ; Max generations count G ;
 $P \leftarrow$ Randomly generate N trees;
for $g = 1$ to G **do**
 $\text{Fit} \leftarrow$ Evaluate fitness values of P ;
 if $\max(\text{Fit}) \geq f_{\text{target}}$ **then**
 break
 end if
 $C \leftarrow$ The empty population.
 while Not enough trees in C **do**
 $\text{Parent1}, \text{Parent2} \leftarrow$ Select parents;
 $\text{Child} \leftarrow$ Crossover($\text{Parent1}, \text{Parent2}$);
 $\text{Child} \leftarrow$ Mutation(Child);
 $C \leftarrow C \cup \{\text{Child}\}$
 end while
end for
return $P[\arg \max(\text{Fit})]$

mance compared to CPUs. This makes handling variable-sized data structures, such as trees, particularly challenging [52].

Compute Unified Device Architecture (CUDA) is a parallel computing platform and programming model developed by NVIDIA, designed to harness the computing power of GPUs for general purpose computing [53], [54]. One of the fundamental execution models in CUDA is SIMT [55]. CUDA organizes parallel execution in a hierarchical manner, consisting of three key levels: grid, block, and thread. A CUDA kernel launches a grid of thread blocks, where each block contains multiple threads. These threads execute in parallel, and the execution is coordinated through shared memory, synchronization mechanisms, and optimizations of the memory hierarchy [45], [56].

C. Existing TGP Implementations

Several TGP libraries have been developed in the past decade, exhibiting varying levels of computational efficiency, scalability, and extensibility.

DEAP [27] and gplearn [28] are representative CPU-based libraries for genetic programming. DEAP is designed for extensibility and supports a wide range of evolutionary algorithms with customizable operators and multiprocessing, whereas gplearn focuses on symbolic regression and classification and employs joblib to parallelize evaluations across CPU cores. In contrast, Operon [29] is a modern CPU-based library that incorporates advanced parallel computing techniques to improve computational efficiency. Its C++ implementation exploits population-level parallelism through Taskflow [57] and data-level parallelism through SIMD vectorization, which provides notable acceleration compared with earlier CPU-based GP libraries.

To improve computational efficiency, several libraries have sought to take advantage of GPU acceleration. KarooGP [33] and TensorGP [34] are built on the TensorFlow framework. KarooGP constructs static computation graphs for each GP individual and executes them using TensorFlow’s graph execution model. This design incurs substantial overhead due to repeated compilation, significantly slowing down execution. TensorGP adopts eager execution to avoid compilation, but still lacks fine-grained control over GPU resources. Combined with Python-level overhead and TensorFlow’s abstraction cost, the resulting performance remains suboptimal.

SRGPU [35] instead implements core operations directly in CUDA for higher performance. Its design allows GPU threads to process all data points for a single individual in parallel, efficiently exploiting data-level parallelism. However, operations such as evaluation, selection, crossover, and mutation are still executed sequentially at the population level, leaving the majority of GPU concurrency untapped and limiting scalability. Furthermore, since SRGPU lacks Python bindings, it cannot be easily integrated into mainstream machine learning or robotics pipelines, which significantly limits its extensibility beyond symbolic regression tasks.

In addition, most existing libraries represent GP trees using traditional pointer-based or chain-like structures. While such representations are sufficient for serial execution within

individuals, they are fundamentally unsuited for efficient population-level parallelism on GPUs. Their irregular and non-contiguous memory layout prevents memory coalescing and hinders the use of fast shared memory, resulting in inefficient global memory access and degraded throughput when scaling parallel execution across individuals.

III. METHODOLOGY

In this section, we present the methodology underlying EvoGP for enabling efficient population-level parallelism in TGP for GPU acceleration. Specifically, we detail the key techniques that address the structural heterogeneity of individuals, support scalable genetic operations, and dynamically optimize GPU utilization.

A. Tensorized Data Structures

To enable efficient population-level parallelism on GPUs, it is important to consider tree representations that allow for coalesced memory access and uniform tensor shapes. As discussed in Section II-C, traditional pointer-based or chain-like structures are inadequate for this setting due to their irregular memory layout and poor compatibility with batched GPU execution.

To overcome these limitations, we adopt a linear prefix encoding scheme that represents each tree as a flat sequence of nodes. In general, prefix sequences alone are insufficient to fully represent arbitrary tree structures, as the number of children per node may vary. However, this ambiguity can be resolved in TGP, where the number of children for each node is entirely determined by its type (t) and its value (val). For instance, *Constant* and *Variable* nodes have no children, whereas a *Unary Function* node (e.g., \sin) has one child, and a *Binary Function* node (e.g., sum) has two children. Consequently, for TGP trees, the prefix sequence of node types and values can encode all critical information about the topology and values of a tree. This allows for a concise, linear representation of arbitrarily structured trees.

Based on this observation, we encode each tree T using two arrays first:

$$\begin{aligned} \mathbf{n}_{\text{type}} &= [t_1, t_2, \dots, t_n] \in \mathbb{N}^{\text{len}(T)}, \\ \mathbf{n}_{\text{val}} &= [val_1, val_2, \dots, val_n] \in \mathbb{R}^{\text{len}(T)}, \end{aligned}$$

where t_i and val_i represent the type and value of the i -th node, respectively, and $\text{len}(T)$ denotes the total number of nodes in the tree T . Although this representation is compact, it does not store explicit structural information. As a result, genetic operations such as subtree crossover and mutation typically require repeatedly parsing the prefix sequence to determine subtree boundaries, which incurs a time complexity of $\mathcal{O}(n)$ and leads to inefficient GPU execution.

To remedy this, we introduce an additional array that records the size of each subtree:

$$\mathbf{n}_{\text{size}} = [\text{size}(1), \text{size}(2), \dots, \text{size}(n)] \in \mathbb{N}^{\text{len}(T)},$$

where $\text{size}(i)$ indicates the size of the subtree rooted at the i -th node. With this information, the boundaries of subtrees can

be directly accessed in $\mathcal{O}(1)$ time, effectively eliminating the need for costly structural parsing and significantly improving the efficiency of GPU-based genetic operations.

Although prefix encoding provides a suitable representation for trees in TGP, it remains challenging to efficiently batch-process these structures on GPUs due to their variable sizes. To address this, we introduce a hyperparameter $|T|_{\max}$, which denotes the maximum allowed number of nodes in a tree. Each of the arrays \mathbf{n}_{type} , \mathbf{n}_{val} , and \mathbf{n}_{size} is then padded with NaN values to form fixed-length arrays:

$$\begin{aligned}\hat{\mathbf{n}}_{\text{type}} &= [t_1, t_2, \dots, \text{NaN}, \dots, \text{NaN}] \in \mathbb{N}^{|T|_{\max}}, \\ \hat{\mathbf{n}}_{\text{val}} &= [\text{val}_1, \text{val}_2, \dots, \text{NaN}, \dots, \text{NaN}] \in \mathbb{R}^{|T|_{\max}}, \\ \hat{\mathbf{n}}_{\text{size}} &= [\text{size}(1), \text{size}(2), \dots, \text{NaN}, \dots, \text{NaN}] \in \mathbb{N}^{|T|_{\max}}.\end{aligned}$$

Here, the actual tree data occupy the first $\text{len}(T)$ positions, and the remaining entries are filled with NaN. This padding strategy ensures that all trees share a consistent tensor shape, enabling straightforward GPU-friendly batching.

Once each tree is converted to padded arrays $\hat{\mathbf{n}}_{\text{type}}$, $\hat{\mathbf{n}}_{\text{val}}$, and $\hat{\mathbf{n}}_{\text{size}}$, we concatenate them across the population dimension. Let P be the total number of trees in the population. Then, the population can be represented using three tensors:

$$\begin{aligned}P_{\text{type}} &= [\hat{\mathbf{n}}_{\text{type}}^1, \hat{\mathbf{n}}_{\text{type}}^2, \dots] \in \mathbb{N}^{P \times |T|_{\max}}, \\ P_{\text{val}} &= [\hat{\mathbf{n}}_{\text{val}}^1, \hat{\mathbf{n}}_{\text{val}}^2, \dots] \in \mathbb{R}^{P \times |T|_{\max}}, \\ P_{\text{size}} &= [\hat{\mathbf{n}}_{\text{size}}^1, \hat{\mathbf{n}}_{\text{size}}^2, \dots] \in \mathbb{N}^{P \times |T|_{\max}},\end{aligned}$$

where $\hat{\mathbf{n}}_{\text{type}}^i$, $\hat{\mathbf{n}}_{\text{val}}^i$, and $\hat{\mathbf{n}}_{\text{size}}^i$ are the padded arrays corresponding to the i -th tree. By unifying all trees into these fixed-shape tensors, genetic operators and fitness evaluations can be designed to leverage GPU parallelism effectively.

Fig. 2 provides a graphical overview of this tensorized encoding scheme. In summary, storing the subtree size array alongside prefix-encoded values enables rapid access to individual subtrees, while padding to a fixed length circumvents the overhead of dynamic memory allocation and irregular indexing on GPUs. As a result, this approach paves the way for an efficient and scalable implementation of TGP that fully exploits modern GPU architectures.

B. Tensorized Operations

The tensorized tree encoding introduced in Section III-A provides not only the basis for efficient batched evaluation, but also a unified structural representation that facilitates high-performance genetic operations on the GPU. Using this encoding, EvoGP supports crossover and mutation entirely on-device, enabling full GPU acceleration throughout the entire evolutionary process.

A key observation is that many widely used genetic operators in tree-based GP, such as one-point crossover, subtree mutation, and hoist mutation, share a common structural primitive: replacing a subtree at a given node with another. This motivates a generalized formulation referred to as *subtree exchange*, which captures the essential transformation underlying a broad class of genetic operations.

Formally, we define the subtree exchange operation as

$$\text{exchange}(T_{\text{old}}, k, T_{\text{new}}) \rightarrow T^*,$$

where T_{old} is the original tree for the subtree exchange, k denotes the root of the target subtree in T_{old} , and T_{new} is the subtree that will replace the original subtree rooted at k . Under our tensorized encoding, each tree is represented by three tensors: \mathbf{n}_{type} , $\mathbf{n}_{\text{value}}$, and \mathbf{n}_{size} . We use \oplus to denote the tensor concatenation operation, and define

$$\begin{aligned}\mathbf{n}_{\text{type}}^* &= \mathbf{n}_{\text{type}}^{\text{old}}[1, 2, \dots, s-1] \oplus \mathbf{n}_{\text{type}}^{\text{new}} \oplus \mathbf{n}_{\text{type}}^{\text{old}}[e, e+1, \dots], \\ \mathbf{n}_{\text{value}}^* &= \mathbf{n}_{\text{value}}^{\text{old}}[1, 2, \dots, s-1] \oplus \mathbf{n}_{\text{value}}^{\text{new}} \oplus \mathbf{n}_{\text{value}}^{\text{old}}[e, e+1, \dots], \\ \mathbf{n}_{\text{size}}^* &= \mathbf{n}_{\text{size}}^{\text{updated}}[1, 2, \dots, s-1] \oplus \mathbf{n}_{\text{size}}^{\text{new}} \oplus \mathbf{n}_{\text{size}}^{\text{old}}[e, e+1, \dots],\end{aligned}$$

where $s = \text{index}(k)$ and $e = s + \mathbf{n}_{\text{size}}^{\text{old}}[k]$ denote the starting and ending positions, respectively, of the original subtree in T_{old} .

The tensor $\mathbf{n}_{\text{size}}^{\text{updated}}$ is computed by adding $\Delta n = \mathbf{n}_{\text{size}}^{\text{new}}[1] - \mathbf{n}_{\text{size}}^{\text{old}}[k]$ to the subtree sizes of all ancestor nodes of k :

$$\mathbf{n}_{\text{size}}^{\text{updated}}[i] = \begin{cases} \mathbf{n}_{\text{size}}^{\text{old}}[i] + \Delta n, & \text{if } i \text{ is an ancestor of } k, \\ \mathbf{n}_{\text{size}}^{\text{old}}[i], & \text{otherwise.} \end{cases}$$

In particular, if $\mathbf{n}_{\text{size}}^{\text{old}}[1] + \Delta n$ exceeds the predefined maximum size constraint, the subtree exchange operation will be considered invalid and the original tree T_{old} will be returned directly. This check is made efficient by maintaining the explicit subtree size array in our tensorized representation.

By focusing on subtree exchange, we can efficiently implement virtually all TGP genetic operations. For instance, the one-point crossover, a fundamental crossover variant, replaces a random subtree of one parent with a random subtree from the other parent:

$$T^* = \text{exchange}(T_1, k, T_2^{\text{sub}}),$$

where T_1 and T_2 are parent trees, k is a random node in T_1 , and T_2^{sub} is a randomly selected subtree from T_2 .

Similarly, subtree mutation replaces a randomly selected subtree with a newly generated subtree:

$$T^* = \text{exchange}(T, k, T_{\text{new}}),$$

where T is the tree to be mutated, k is a random node in T , and T_{new} denotes the newly generated subtree. Fig. 3 provides a graphical overview of these operations and their corresponding transformations in the tensorized encoding.

Once subtree exchange is implemented as a GPU primitive, many genetic operators can be realized by simply changing how subtrees are selected or constructed. Since the core tensor manipulation logic remains unchanged, new operator variants can be added without modifying the GPU kernel itself. This design streamlines the development of new algorithms and ensures that all genetic operations benefit from high-throughput GPU execution. As a result, the method delivers both high performance and broad extensibility across genetic operators.

C. Adaptive Parallelism in Fitness Evaluation

Symbolic regression (SR) [13]–[16] is a central application of TGP, where each individual’s fitness is computed by comparing its predicted outputs against target values across all data points in a dataset. To ensure high GPU utilization across datasets of varying sizes, EvoGP introduces an *adaptive*

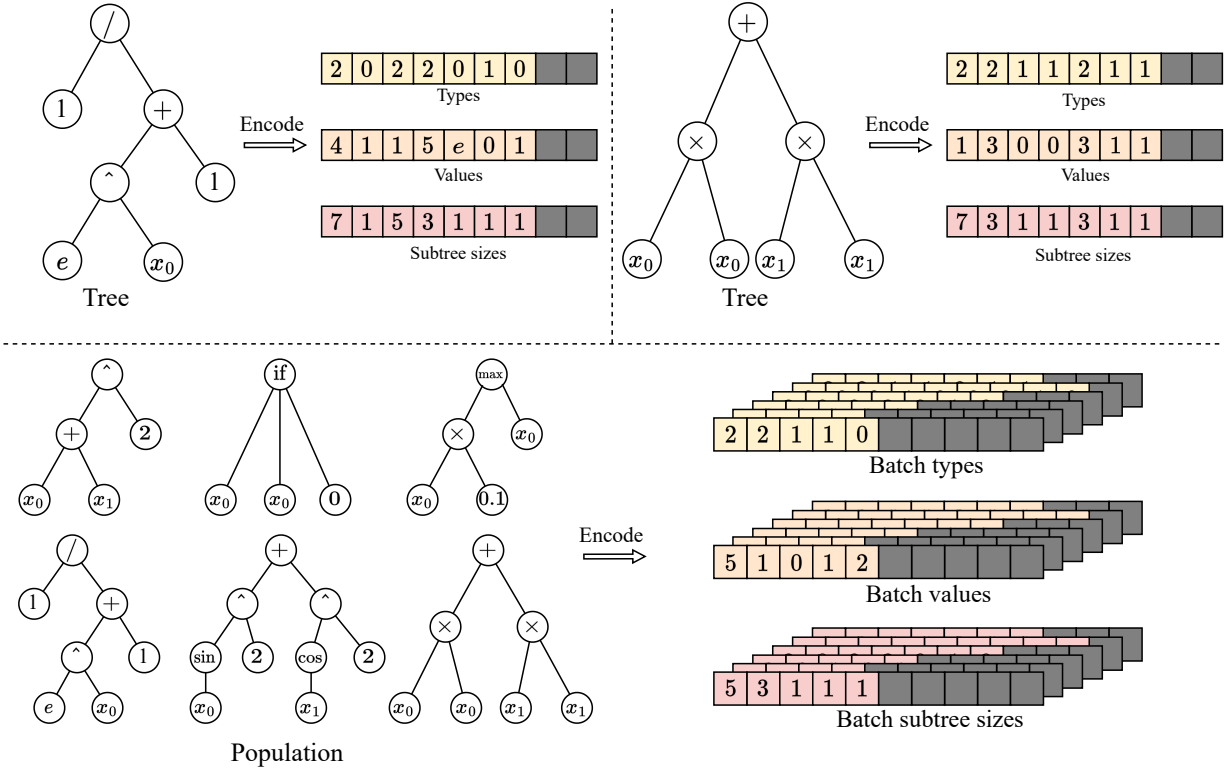


Fig. 2: Illustration of the tree encoding process. In tensorized encoding, a tree is encoded into three tensors: types, values, and subtree sizes. We use NaN padding to ensure that these tensors reach a uniform maximum size, allowing trees of different structures to be encoded into tensors of the same shape. This enables the encoding of an entire population of trees into three batched tensors.

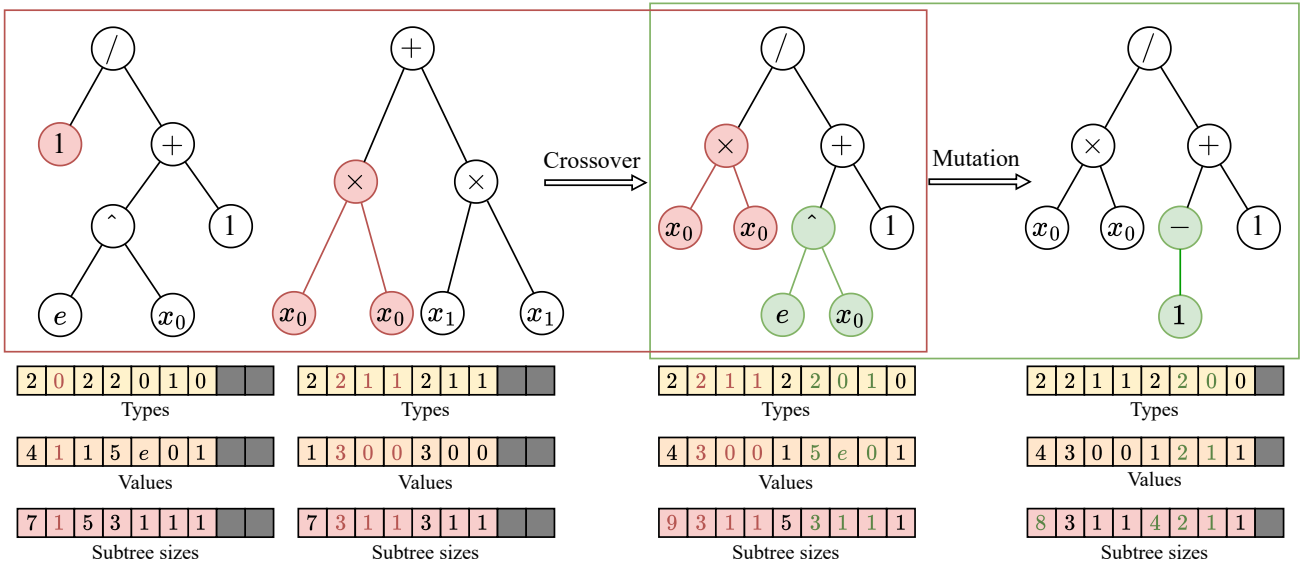


Fig. 3: An illustration of genetic operations in TGP. The upper part depicts the structural modifications of trees. The red box highlights the crossover operation, where two parent trees exchange subtrees to generate a new tree. The green box illustrates the mutation process, where a subtree of a given tree is replaced with a newly generated subtree. The lower part of the figure demonstrates the corresponding transformations in the tensor representation of trees for both crossover and mutation operations.

parallelism strategy that dynamically selects the appropriate execution mode at runtime.

When the number of data points D is small to moderate, evaluating a single individual alone does not fully saturate the GPU. To avoid under-utilization, EvoGP adopts a hybrid parallelism strategy that combines data-level and population-level parallelism within a single kernel launch. Specifically, it configures a two-dimensional CUDA grid of shape $(P, \text{block_cnt})$, where P is the population size and each block processes a segment of data points for a given tree:

$$\begin{aligned} \text{block_size} &= \min(D, 1024), \\ \text{block_cnt} &= \left\lceil \frac{D}{\text{block_size}} \right\rceil. \end{aligned}$$

In this configuration, multiple CUDA blocks are assigned to evaluate each individual, with each block independently computing a partial fitness result over its assigned data segment. These partial results are subsequently aggregated using hardware-supported atomic operations to ensure a correct and efficient fitness accumulation. This hybrid parallelization strategy improves GPU utilization even when D is relatively small, as inter-individual parallelism compensates for the limited workload per individual. Additionally, performing the entire evaluation in a single kernel launch minimizes the launch overhead and further improves the computational efficiency. Fig. 4 (top right) illustrates this mode.

However, as the dataset size increases, the evaluation of a single individual on D data points may already saturate all available CUDA cores. In such cases, adding population-level parallelism offers little to no additional benefit in GPU utilization. EvoGP therefore switches to a pure data-level parallelism strategy, where each individual’s evaluation is launched in a separate kernel invocation. The purpose of this shift is to optimize memory access by loading the individual’s tree into constant memory before the kernel launch. Since

constant memory is immutable during execution but offers fast broadcast access across threads, this approach greatly accelerates memory reads during evaluation. Compared to the hybrid scheme, where trees are accessed from slower global memory, the constant memory design significantly improves memory throughput and overall runtime efficiency for large-scale workloads. Fig. 4 (bottom right) illustrates this mode.

To support both cases without manual configuration, EvoGP integrates a runtime switching mechanism, referred to as *Choose Parallelism Adaptively*, which selects the appropriate execution strategy based on the dataset size. The switching threshold is determined by comparing the number of data points D with the total number of CUDA cores, estimated from the number of Streaming Multiprocessors (SMs) and their count of cores per SM. Section V-B further examines how their performance varies with dataset size and, based on these results, investigates the trade-off between the two strategies.

Regardless of the parallelism scheme selected, the computation of a single individual’s output follows the standard stack-based evaluation of a postfix (reverse Polish) expression. Although each tree is stored in a prefix-encoded format, the computation is carried out in reverse order, effectively simulating a postfix traversal. The total tree length is obtained from $\mathbf{n}_{\text{size}}[0]$, and nodes are processed from end to start. At each step, the node’s arity is inferred from its type, and its output is computed by applying the corresponding operation to values on the evaluation stack. This execution pattern is naturally compatible with the prefix encoding format, making it particularly suitable for efficient implementation on GPUs.

IV. IMPLEMENTATION

In this section, we present the overall system architecture of EvoGP, detailing its core design components and implementation features. Specifically, we describe how the framework integrates GPU-accelerated operations with high-level

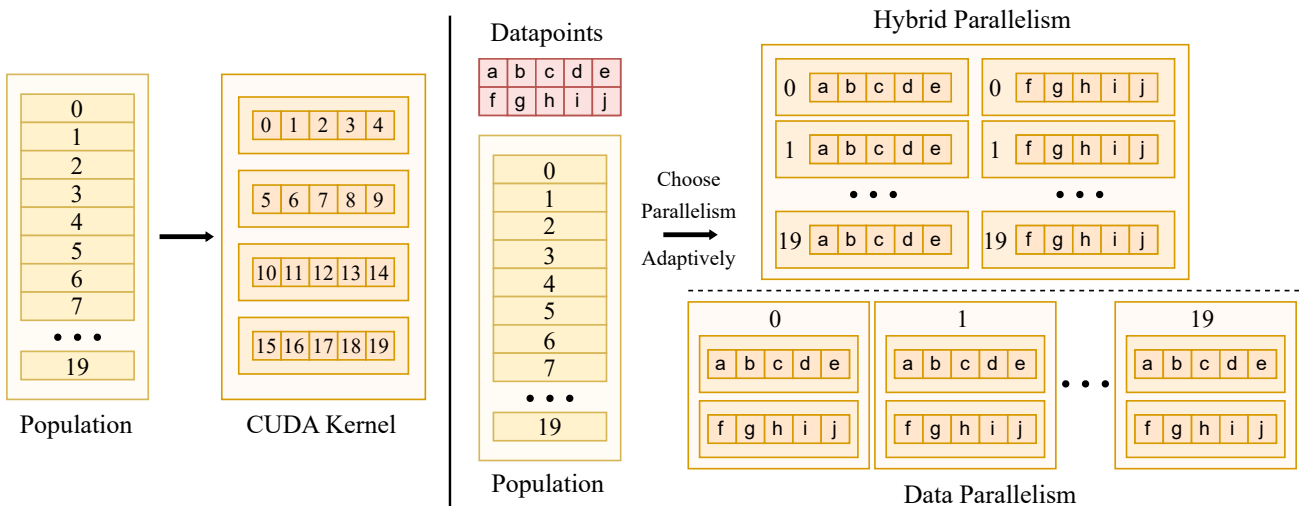


Fig. 4: Illustration of CUDA-based parallelism in EvoGP. **Left:** Population parallelism for generation, crossover, mutation and inference kernel, where each individual is assigned to a separate thread. **Right:** SR fitness evaluation, with hybrid parallelism (upper) computing all trees in one kernel launch, while data parallelism (lower) processes each tree separately across multiple launches. The system adaptively switches between the two modes based on dataset size.

Python interfaces, and highlight several additional capabilities that enhance its usability, flexibility, and support for diverse application scenarios.

A. Overview of EvoGP

The overall system architecture of EvoGP is depicted in Fig. 5, which illustrates its modular components and their interactions. Specifically, EvoGP is implemented in Python and leverages the PyTorch framework [44] for efficient tensor manipulation and GPU resource management.

To optimize computational performance, EvoGP incorporates a suite of custom CUDA kernels for critical evolutionary operations, including tree initialization, mutation, crossover, inference, and fitness evaluation in symbolic regression (SR) tasks. To accommodate input datasets of varying sizes during SR evaluation, EvoGP adopts both data-parallel and hybrid-parallel execution strategies, as detailed in Section III-C. These CUDA kernels are integrated into the PyTorch runtime as custom operators, enabling seamless compatibility with the broader PyTorch ecosystem.

Complementing these kernel-level optimizations, EvoGP adopts a model for full-GPU residency, which ensures that data is not frequently transferred between the host and the device. By maintaining both the population and the evaluation context entirely on the GPU, EvoGP effectively eliminates the substantial communication overhead typical of traditional frameworks. This zero-copy design philosophy facilitates compatibility with modern reinforcement learning environments that are GPU-accelerated. Consequently, the architecture enables parallel simulations that are both efficient and end-to-end, thereby eliminating potential IO bottlenecks. Collectively, this design integrates the flexibility of Python-based development with the high-throughput capabilities of GPU acceleration, thereby ensuring that EvoGP is accessible and computationally efficient.

In addition to accelerating TGP algorithms, EvoGP includes built-in support for several representative application domains, including symbolic regression, policy optimization, and classification. It also provides a curated set of standardized benchmarks across these domains, facilitating systematic evaluation of different TGP variants and enabling fine-grained algorithmic tuning.

B. Rich Features and User Customization

EvoGP extends beyond basic GPU-accelerated TGP operations by offering a diverse set of evolutionary operator variants and a flexible interface for customization. In addition to the problem benchmarks mentioned above, EvoGP provides multiple variations of key TGP operators, including selection, mutation, and crossover. These variants allow users to freely combine and configure different evolutionary strategies, enabling the design of customized TGP algorithms tailored to specific optimization tasks. Table I compares the range of operator variants implemented in the main TGP libraries, highlighting that EvoGP provides the comprehensive set of supported operators.

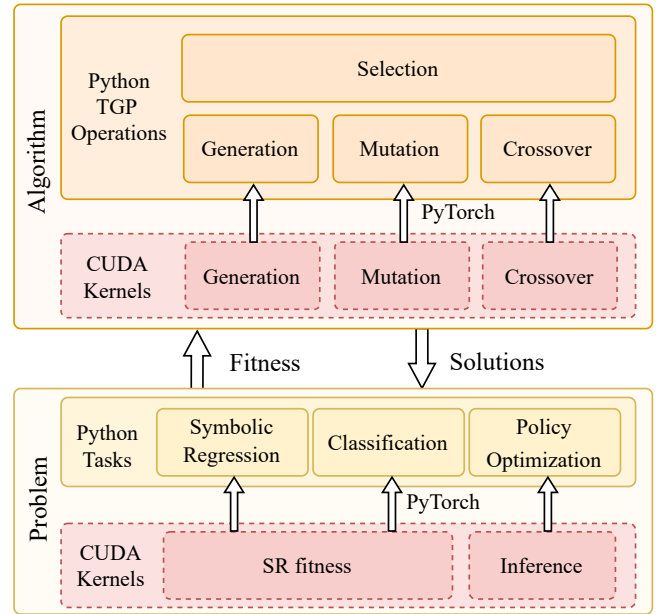


Fig. 5: Illustration of the EvoGP architecture. EvoGP consists of two main components: Algorithm and Problem. The Algorithm module implements the TGP algorithm along with multiple operation variants. The Problem module integrates various benchmark problems for user evaluation. Within these components, we design CUDA kernels to enable parallel acceleration of computational processes. These CUDA kernels are seamlessly integrated into Python using PyTorch’s custom operator functionality.

To further enhance usability, EvoGP offers an intuitive interface for defining custom operators and problem formulations. Users can leverage low-level CUDA implementations to efficiently develop and execute their own optimized genetic operators, ensuring high performance while maintaining flexibility. Additionally, EvoGP’s modular design allows researchers and practitioners to apply TGP algorithms to their own problem domains, making it a versatile tool for both academic research and real-world applications.

C. Multi-Output Support

EvoGP extends traditional TGP by incorporating multi-output functionality, allowing the application of TGP to tasks that require multiple output values, such as policy optimization in reinforcement learning. This enhancement enables EvoGP to handle complex problem domains where a single-output GP framework would be insufficient.

To achieve multi-output computation, EvoGP uses Modi nodes [58] in the tree structure. These nodes possess two key characteristics:

- 1) Each Modi node specifies the output to which its value contributes. The contributions from multiple Modi nodes associated with the same output are aggregated according to a predefined rule, which in this case is summation, to produce the final output value.
- 2) If a Modi node has a parent node, it does not propagate its computed value upward like regular nodes. Instead,

TABLE I
COMPARISON OF MUTATION AND CROSSOVER OPERATORS IN GENETIC PROGRAMMING TOOLS

Name	One Point Cross.	One Point Leaf Biased Cross.	Subtree Mut.	Hoist Mut.	Single Point Mut.	Multi-Point Mut.	Insert Mut.	Delete Mut.	Single Const Mut.	Multi-Const Mut.
DEAP	✓	✓	✓	×	✓	×	✓	✓	✓	✓
Gplearn	✓	×	✓	✓	✓	×	×	×	×	×
KarooGP	✓	×	✓	×	✓	×	×	×	×	×
TensorGP	✓	×	✓	×	✓	×	✓	✓	×	×
SRGPU	✓	×	✓	✓	✓	✓	×	×	×	×
EvoGP (Ours)	✓	✓	✓	✓	✓	✓	✓	✓	✓	✓

it directly adopts the value of its rightmost child node. This mechanism effectively transforms the tree structure into a directed acyclic graph (DAG), enabling the simultaneous computation of multiple outputs.

This distinction between regular nodes and Modi nodes is crucial when performing multi-output computations. Although regular nodes operate under standard GP rules, Modi nodes follow a specialized processing scheme to ensure proper output assignment. This approach enables EvoGP to effectively support multi-output GP, making it well-suited for reinforcement learning and other tasks requiring multiple correlated outputs. The computational logic of Modi nodes is illustrated in Fig. 6, which provides a schematic view of how multiple outputs are generated and propagated within the EvoGP framework.

V. EXPERIMENTS

In this section, we evaluate the performance of EvoGP across a broad range of tasks and datasets. The experiments are designed to verify the effectiveness of the proposed GPU-accelerated framework in addressing the computational challenges inherent in TGP. Specifically, the evaluations aim to answer the following questions: (1) How do hybrid and data-level parallelism perform under different conditions, and how should the switching threshold be determined according to hardware and workload characteristics? (2) How does

EvoGP compare with existing implementations in terms of execution performance and solution quality, while simultaneously validating its scalability with respect to population size? (3) How does EvoGP perform across different application domains, including symbolic regression, classification, and robotics control? Addressing these questions demonstrates the efficiency, scalability, and adaptability of EvoGP across diverse computational scenarios.

A. Experimental Setup

This section presents the experimental configuration used to evaluate the performance of EvoGP. All experiments were executed on a high-performance workstation, whose hardware specifications are summarized in Table II. Standard TGP parameter settings commonly adopted in the literature were employed. To rigorously assess performance, key hyperparameters (i.e., population size and number of data points) were systematically varied, whereas the remaining parameters were fixed as listed in Table III. Each experiment was independently repeated ten times with distinct random seeds to ensure statistical robustness. The reported results are given as mean values with 95% confidence intervals, providing a consistent and reliable basis for evaluating the efficiency, scalability, and adaptability of EvoGP.

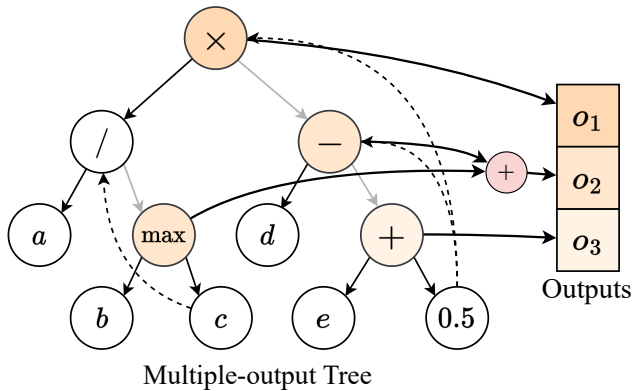


Fig. 6: An example of a multiple-output tree. The yellow nodes at different depths represent the Modi nodes. Each Modi node adds its value to the corresponding position in the output and propagates the value of its rightmost subtree to its parent node. The computed process in the figure are: $o_1 = a \div c \times 0.5$, $o_2 = \max(b, c) + (d - 0.5)$, $o_3 = e + 0.5$.

TABLE II
HARDWARE SPECIFICATIONS

Component	Specification
CPU	Intel(R) Xeon(R) Gold 6226R
CPU Cores	32
GPU (Section V-B)	NVIDIA RTX 3090
GPU (Sections V-C & V-D)	NVIDIA RTX 4090
Host RAM	512 GB
GPU RAM	24 GB
OS	Ubuntu 22.04.4 LTS

TABLE III
CONFIGURATION OF GENETIC PROGRAMMING

Parameter	Value
Maximum Tree Size	512
Generations	100
Tournament Size	20
Crossover Probability	0.9
Mutation Probability	0.1
Function Set	{+, -, ×, ÷, sin, cos, tan}

B. Threshold Analysis for Adaptive Parallelism

To validate the effectiveness of EvoGP’s adaptive parallelism strategy, we conducted an experiment to identify the optimal threshold for switching between hybrid and data-level parallelism. This analysis was performed using a symbolic regression task benchmarked on the Pagie polynomial, a widely used non-linear function in GP research defined as:

$$f(x, y) = \frac{1}{1 + x^{-4}} + \frac{1}{1 + y^{-4}}.$$

Fig. 7 presents the wall-clock execution time as a function of the number of data points (x-axis) for four population sizes: 100, 1,000, 5,000, and 10,000. The y-axis denotes the average execution time in seconds. Across all configurations, a consistent performance trend is observed: hybrid parallelism yields lower execution time when the dataset is small, while data-level parallelism becomes more efficient as the dataset grows. This crossover behavior reflects the GPU utilization characteristics described in Section III-C. When the number of data points is insufficient to fully occupy the GPU via data-level execution alone, hybrid parallelism leverages population-level concurrency to fill idle cores. As the dataset size increases, evaluating a single individual becomes sufficient to saturate the device, making population-level parallelism redundant. In this case, data-level parallelism further benefits from constant memory access, which provides faster broadcast capabilities than the global memory used in hybrid execution.

Although $D = 16,384$ is the first experimental point at which data-level parallelism visibly outperforms hybrid parallelism, the actual crossover appears to occur closer to $D \approx 10,496$. This value coincides with the total number of CUDA cores on the NVIDIA GeForce RTX 3090, which has 82 streaming multiprocessors with 128 cores each, totaling $82 \times 128 = 10,496$. This alignment suggests that data-level parallelism becomes more effective once the dataset size is large enough to fully utilize GPU’s computational resources without requiring additional population-level work.

These findings provide empirical support for EvoGP’s runtime switching mechanism, which selects the parallelism strategy by comparing the dataset size against the total number of available CUDA cores. By grounding this decision in hardware-aware thresholds, EvoGP dynamically adapts to diverse computational workloads and consistently maintains high execution efficiency.

C. Comparison with Existing TGP Implementations

To benchmark the performance of EvoGP, we selected several representative libraries for comparison. For CPU-based frameworks, we considered three established TGP libraries: DEAP [27], gplearn [28], and Operon [29]. Since Operon provides alternative mathematical backends that affect performance results, we utilized the Eve backend to enhance computational throughput. For GPU-based counterparts, we included SRGPU [35]. Furthermore, PySR [59] was incorporated as an additional reference. A supplementary comparison with the TensorGP GPU library [34] is provided in Section S.I of the Supplementary Document. All benchmarks were performed on

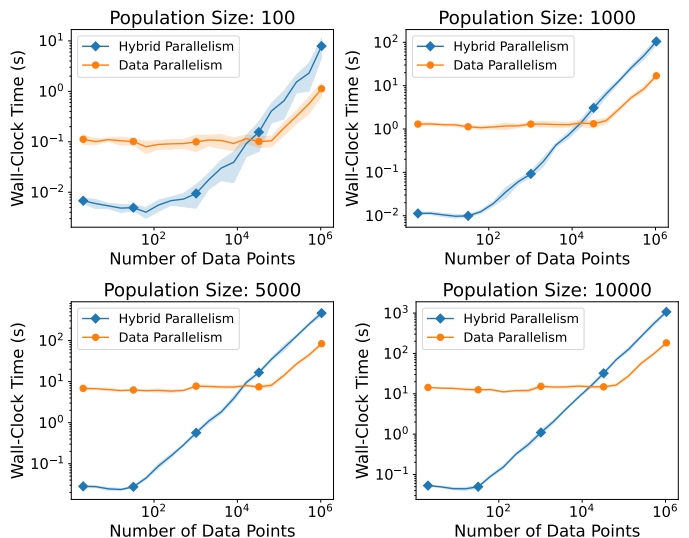


Fig. 7: Parallelism performance in terms of the number of data points.

four symbolic regression tasks collected from diverse sources. These tasks include Daily Demand Forecasting and Auto MPG from the UCI Machine Learning Repository [60], California Housing from scikit-learn [61], and Feynman I.9.18 from the Feynman Symbolic Regression Database [62]. Detailed specifications of these tasks are summarized in Table IV. Each experiment was executed for 100 generations. To ensure a consistent comparative timeframe, we only present results for the runs that completed within one hour.

TABLE IV
DETAILS OF SYMBOLIC REGRESSION DATASETS FROM THE UCI REPOSITORY

Dataset	Input Features	Data Count
Daily Demand Forecasting [63]	12	60
Auto MPG [64]	7	398
California Housing [65]	8	20,640
Feynman I.9.18 [62]	9	100,000

As presented in Fig. 8, the experimental results provide a comprehensive comparison of execution time and solution quality across different population sizes and datasets. The top row shows the total execution time as a function of population size and uses a logarithmic scale for each dataset. Across all scenarios EvoGP consistently exhibits markedly lower execution times. While baseline libraries display approximately linear scaling with population size and appear exponential due to the logarithmic axis, EvoGP demonstrates a flatter scaling curve. It maintains nearly constant execution time at smaller population sizes and shows only moderate increases for populations in the hundreds of thousands. The bottom row presents solution quality measured by mean squared error (MSE). EvoGP matches or surpasses the accuracy of competing libraries and confirms that its substantial computational speedup does not come at the expense of solution quality.

While wall-clock time provides a direct measure of speed, Langdon [66] introduced a metric that more precisely reflects the operational throughput of GP systems, termed GP oper-

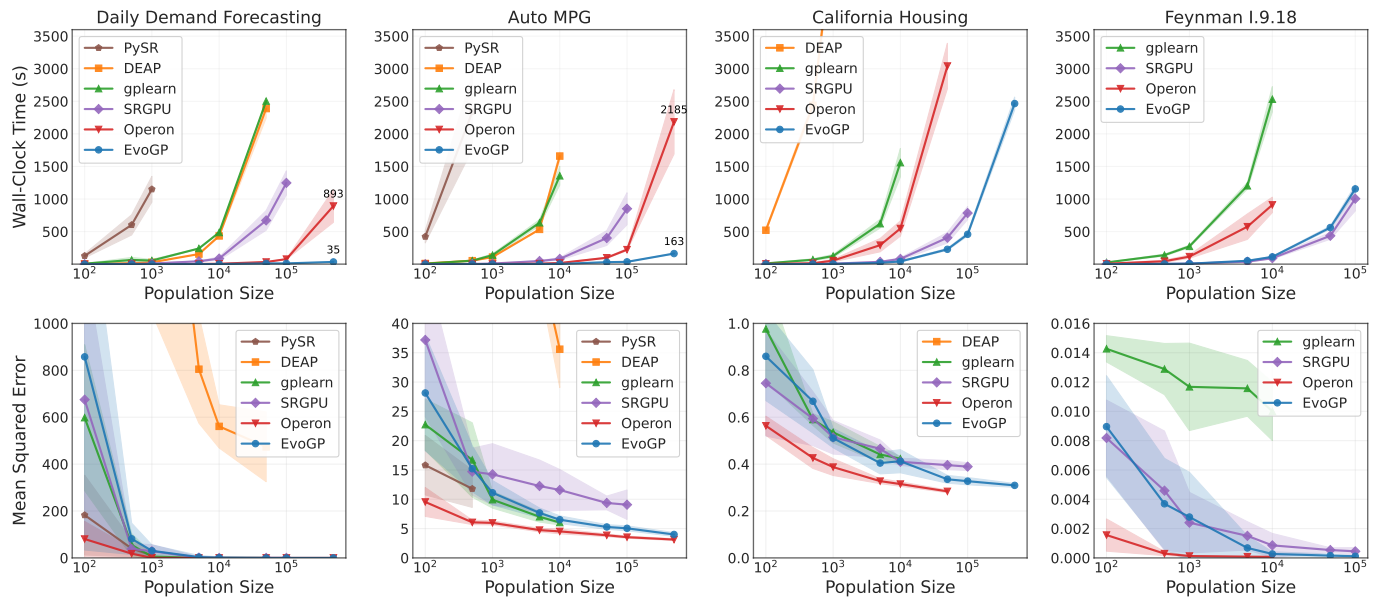


Fig. 8: Comparison with existing TGP implementations on four datasets. The top row presents the total execution time as a function of population size on a logarithmic scale, and the bottom row shows the corresponding solution quality measured by MSE.

ations per second (GPops/s). The GPops/s metric is defined as the total number of genetic program primitive operations evaluated per second across all fitness cases, calculated as:

$$\text{GPops/s} = \frac{G \times P \times \bar{S} \times D}{T},$$

where G denotes the number of generations, P the population size, \bar{S} the average program size measured by the number of nodes, D the number of individual fitness cases (i.e., data points), and T the total execution time in seconds.

EvoGP achieves robust computational throughput, maintaining a magnitude of approximately 10^{10} GPops/s on small datasets and reaching 10^{11} GPops/s on medium-to-large datasets, as detailed in Table V. Based on this high throughput, we compared EvoGP against the leading GPU-based library, SRGPU, and the CPU-based library, Operon, as illustrated in Fig. 9 and Fig. 10. The results indicate that EvoGP holds a substantial performance advantage. Specifically, on smaller problems, EvoGP achieves peak speedups of $304\times$ relative to SRGPU and $18\times$ relative to Operon. In scenarios involving

TABLE V
SUMMARY OF EVOGP GPOPS/S PERFORMANCE ACROSS VARIOUS POPULATION AND DATASET SIZES.

Population Size	GPops/s by Dataset Size (Datapoints)			
	60	392	20,640	100,000
100	2.05×10^8	1.26×10^9	3.49×10^{10}	1.55×10^{11}
500	1.20×10^9	8.67×10^9	1.27×10^{11}	3.35×10^{11}
1,000	1.85×10^9	1.02×10^{10}	1.61×10^{11}	3.50×10^{11}
5,000	7.31×10^9	2.93×10^{10}	2.07×10^{11}	4.14×10^{11}
10,000	1.13×10^{10}	4.32×10^{10}	2.08×10^{11}	3.92×10^{11}
50,000	1.67×10^{10}	3.38×10^{10}	2.14×10^{11}	4.10×10^{11}
100,000	2.27×10^{10}	5.31×10^{10}	2.12×10^{11}	4.05×10^{11}
500,000	3.25×10^{10}	5.87×10^{10}	1.99×10^{11}	3.78×10^{11}
1,000,000	3.29×10^{10}	5.87×10^{10}	1.97×10^{11}	3.90×10^{11}

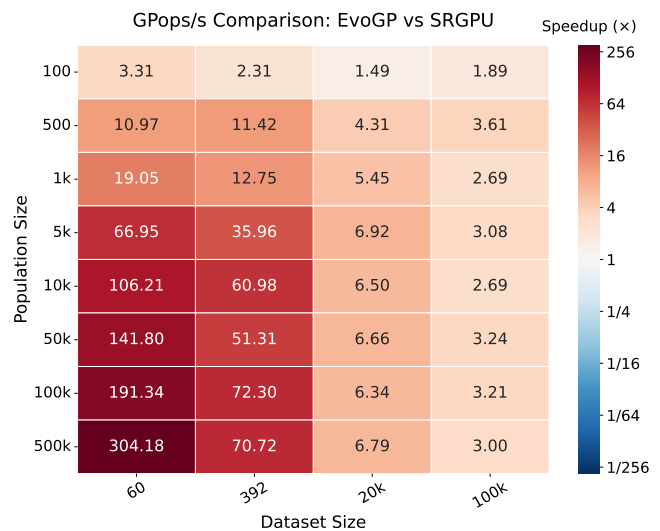


Fig. 9: Heatmap of GPops/s comparison between EvoGP and SRGPU. Each value represents the speedup factor of EvoGP relative to SRGPU across different population sizes and datasets. Red regions indicate cases where EvoGP achieves higher throughput, whereas blue regions indicate cases where SRGPU performs faster.

medium to large datasets, data-point parallelism saturates GPU resources, which naturally constrains the speedup magnitude. Nevertheless, EvoGP maintains a robust lead, thereby delivering at least a $3\times$ speedup over SRGPU. Against Operon, EvoGP sustains an approximately $10\times$ advantage, a margin that becomes particularly pronounced when the population size exceeds 1,000. Although the hardware generational gap favors the GPU (14nm CPU vs. 8nm GPU), the order-of-

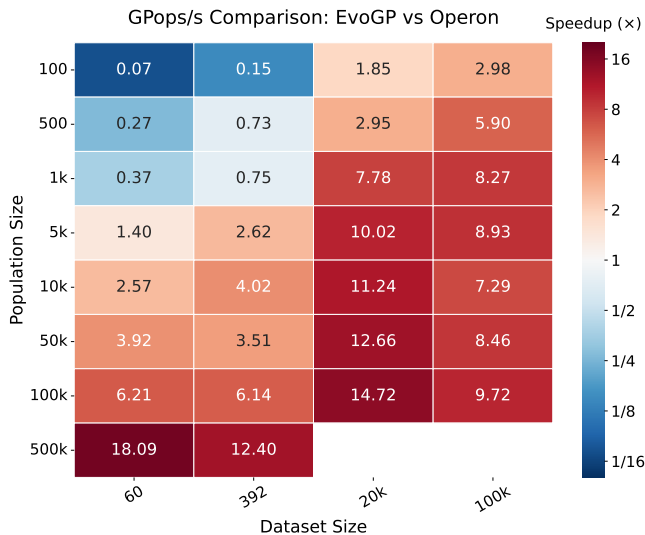


Fig. 10: Heatmap of GPods/s comparison between EvoGP and Operon. Each value represents the speedup factor of EvoGP relative to Operon across different population sizes and datasets. Red regions indicate cases where EvoGP achieves higher throughput, whereas blue regions indicate cases where Operon performs faster.

magnitude speedups achieved by EvoGP remain substantial. Consequently, even with an estimated 40% gain from a more modern 7nm CPU architecture, the throughput advantage of EvoGP remains clearly evident. A detailed breakdown of these results, including the exact GPods/s values for all compared libraries, is provided in Section S.III of the Supplementary Document.

Taken together, these results demonstrate the efficiency and robustness of EvoGP’s GPU-accelerated design. The observed performance gain results from the customized design of EvoGP, which utilizes population-level parallelism while sustaining efficient GPU utilization.

D. Performance in Multiple Tasks with Scalable Populations

We evaluate the performance of EvoGP across three domains: symbolic regression, classification, and robotics control. For all tasks, we test population sizes of 200, 1,000, and 5,000. In symbolic regression, the experiments utilize the benchmarks described in Section V-C and adopt MSE as the performance metric. Specifically, lower values indicate superior accuracy. In classification, we employ four datasets from the UCI repository [60]: *Wine*, *Chronic Kidney Disease*, *Breast Cancer Wisconsin*, and *Yeast*. These datasets exhibit heterogeneity in the number of input features, output classes, and data instances. Table VI summarizes these specifications. We measure performance via classification accuracy, where higher values denote better results. In robotics control, we utilize four environments from the Brax framework [48]: *Swimmer*, *Hopper*, *Walker2d*, and *HalfCheetah*. Table VII lists the observation and action dimensions of these environments. Performance is evaluated by the cumulative reward obtained

TABLE VI
DETAILS OF CLASSIFICATION DATASETS

Dataset	Input Features	Output Classes	Data Count
Wine [67]	13	3	178
Chronic Kidney Disease [68]	24	3	400
Breast Cancer Wisconsin [69]	30	2	569
Yeast [70]	8	10	1484

TABLE VII
DETAILS OF BRAX ENVIRONMENTS

Environment	Observation Dimension	Action Dimension
Swimmer	8	2
Hopper	17	3
Walker2d	17	6
HalfCheetah	17	6

during an episode. Consequently, higher rewards represent improved control effectiveness.

The results are shown in Fig. 11 and Table VIII. The figure presents task performance with respect to wall-clock time and illustrates the convergence behaviour for each population size, whereas summarizes the final performance of each population at the end of the corresponding runtime. A comparison of performance over a fixed number of generations is provided in Section S.IV of the Supplementary Document.

Across all three domains, the results indicate that larger populations yield lower MSE in regression, higher accuracy in classification, and higher cumulative rewards in control tasks. As shown in Table VIII, the improvement is most evident in the HalfCheetah control task, where increasing the population from 200 to 5,000 more than doubled the cumulative reward, and in the Daily Demand Forecasting regression task, where the final MSE decreased by over two orders of magnitude. Similarly, in the Yeast classification task, increasing the population size enabled EvoGP to surpass the standard accuracy of Neural Networks (56.87%) and closely approach the best accuracy reported in the UCI repository

TABLE VIII
PERFORMANCE ACROSS VARIOUS TASKS AND POPULATION SIZES IN THE SAME TIME.

Task Identifier	Population Size		
	200	1,000	5,000
<i>Symbolic Regression (MSE Loss — lower is better)</i>			
Daily Demand Forecasting	374.578	21.330	1.963
Auto MPG	10.790	9.144	7.205
California Housing	0.533	0.451	0.426
Feynman I.9.18	2.207e-3	9.274e-4	7.239e-4
<i>Classification (Accuracy — higher is better)</i>			
Wine	0.823	0.951	0.974
Chronic Kidney Disease	0.943	0.963	0.971
Breast Cancer Wisconsin	0.952	0.973	0.976
Yeast	0.506	0.549	0.591
<i>Robotics Control (Cumulative Reward — higher is better)</i>			
Swimmer	365.0	370.5	372.2
Hopper	1344.7	2274.4	2658.9
Walker2d	1839.5	1958.5	2364.7
Halfcheetah	5781.2	11954.0	13862.9

* The best performances are highlighted in bold.

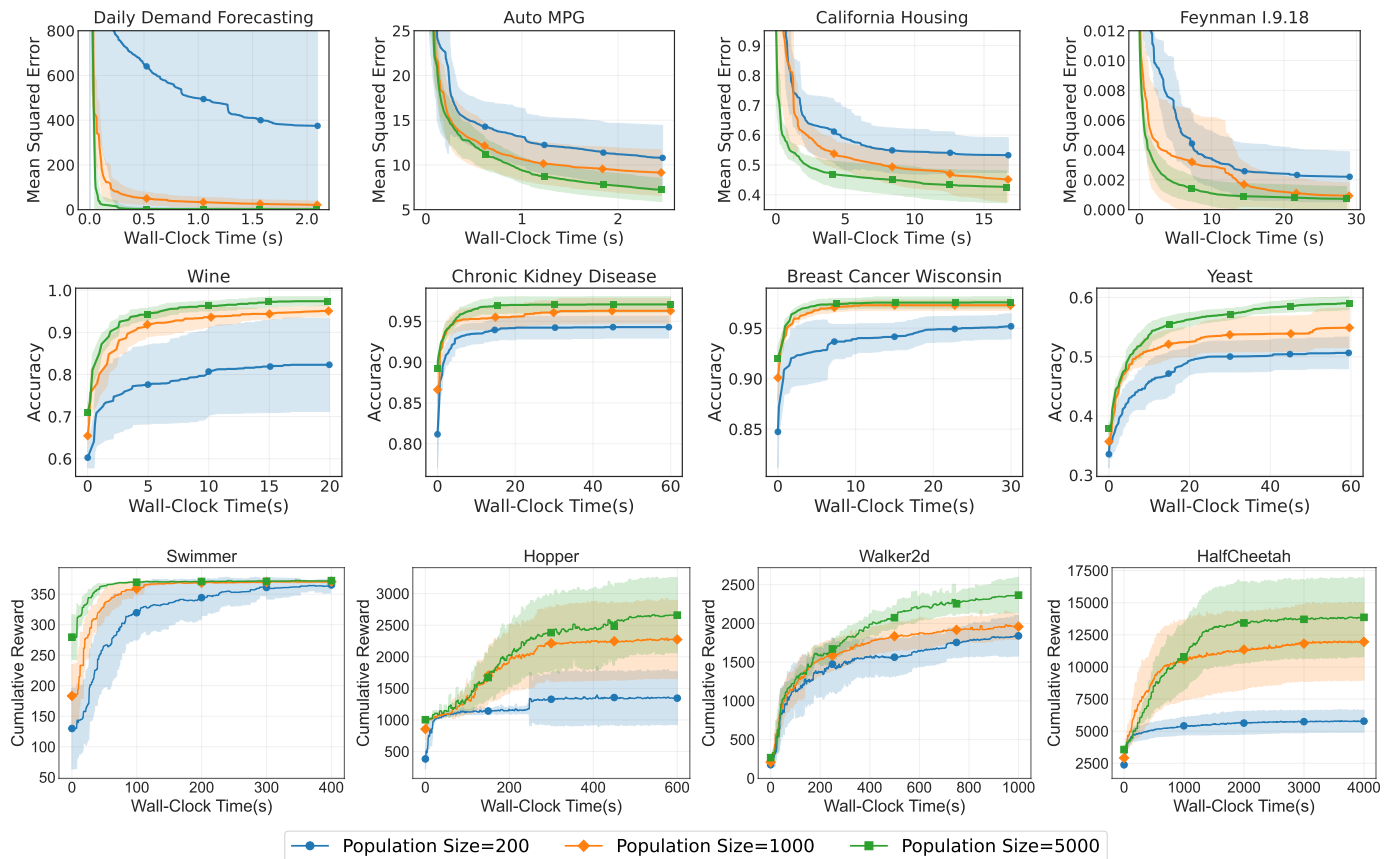


Fig. 11: Task performance versus wall-clock time for various population sizes. Rows correspond to symbolic regression, classification, and robotics control tasks, respectively.

benchmarks (62.80%, achieved by Random Forest). These observations suggest that larger populations may contribute to improved GP performance by enabling more comprehensive explorations of the solution space.

The key factor underlying the performance of large populations lies in EvoGP’s GPU-accelerated population-level parallelism. This mechanism enables scalability without a proportional increase in computation time. As illustrated in Fig. 11, the efficiency of this design allows larger populations to reach higher-quality solutions in less wall-clock time than smaller ones. This property enables EvoGP to outperform CPU-based or sequential implementations in both computational speed and final solution quality.

VI. CONCLUSION

In this paper, we presented EvoGP, a fully GPU-accelerated framework for Tree-based Genetic Programming (TGP) that effectively addresses three fundamental challenges: the structural heterogeneity of individuals, the complexity of combining multiple levels of parallelism, and the tension between high-performance execution and Python-based flexibility. EvoGP introduces a tensorized representation that transforms structurally diverse trees into fixed-shape, memory-aligned arrays, thereby enabling efficient and consistent memory access for population-level GPU execution.

To further enhance evaluation efficiency, we proposed an adaptive parallelism strategy that dynamically fuses intra- and inter-individual parallelism based on dataset size. EvoGP seamlessly integrates with Python environments via custom CUDA operators within the PyTorch runtime, thereby allowing effortless deployment in popular platforms such as Gym and MuJoCo. Experimental results show demonstrate that EvoGP attains a peak throughput exceeding 10^{11} GPops/s, with which corresponds to speedups of up to $304\times$ over GPU-based TGP implementations and $18\times$ over the fastest CPU-based libraries. Furthermore, while EvoGP preserving preserves solution quality and improving improves scalability for large populations.

Looking forward, we aim to extend EvoGP to support more complex and diverse applications. Its computational efficiency and scalable parallelism provide a foundation for utilizing larger and more diverse populations, which can enhance performance in demanding scenarios such as robotic control and autonomous decision-making. While the current implementation supports multi-output tasks, future research will explore more advanced strategies to further enhance expressiveness and generalizability. We envision EvoGP as a robust and extensible framework that empowers researchers to advance the frontiers of interpretable and evolutionary AI.

REFERENCES

- [1] J. R. Koza, "Genetic programming as a means for programming computers by natural selection," *Statistics and Computing*, vol. 4, pp. 87–112, 1994.
- [2] Y. Mei, Q. Chen, A. Lensen, B. Xue, and M. Zhang, "Explainable artificial intelligence by genetic programming: A survey," *IEEE Transactions on Evolutionary Computation*, vol. 27, no. 3, pp. 621–641, 2022.
- [3] S. de Vries, S. W. Keemink, and M. A. van Gerven, "Kozax: Flexible and scalable genetic programming in JAX," 2025. [Online]. Available: <https://arxiv.org/abs/2502.03047>
- [4] J. R. Koza, "Genetic programming: a paradigm for genetically breeding populations of computer programs to solve problems," Stanford University, Stanford, CA, USA, Tech. Rep., 1990.
- [5] W. Banzhaf, F. D. Francone, R. E. Keller, and P. Nordin, *Genetic programming: an introduction: on the automatic evolution of computer programs and its applications*. Morgan Kaufmann Publishers Inc., 1998.
- [6] M. F. Brameier and W. Banzhaf, *Basic concepts of linear genetic programming*. Springer, 2007.
- [7] J. F. Miller, "An empirical study of the efficiency of learning boolean functions using a cartesian genetic programming approach," in *Proceedings of the 1st Annual Conference on Genetic and Evolutionary Computation - Volume 2*, ser. GECCO'99. San Francisco, CA, USA: Morgan Kaufmann Publishers Inc., 1999, p. 1135–1142.
- [8] J. Miller and A. Turner, "Cartesian genetic programming," in *Proceedings of the Companion Publication of the 2015 Annual Conference on Genetic and Evolutionary Computation*, ser. GECCO Companion '15. New York, NY, USA: Association for Computing Machinery, 2015, p. 179–198.
- [9] C. Ferreira, "Gene expression programming: A new adaptive algorithm for solving problems," *Complex Systems*, vol. 13, no. 2, pp. 87–129, 2001.
- [10] M. O'Neill and C. Ryan, "Grammatical evolution," *IEEE Transactions on Evolutionary Computation*, vol. 5, no. 4, pp. 349–358, 2001.
- [11] D. Ari and B. B. Alagöz, "A review of genetic programming: Popular techniques, fundamental aspects, software tools and applications," *Sakarya University Journal of Science*, vol. 25, no. 2, pp. 397–416, 2021.
- [12] D. R. White, J. McDermott, M. Castelli, L. Manzoni, B. W. Goldman, G. Kronberger, W. Jaśkowski, U.-M. O'Reilly, and S. Luke, "Better GP benchmarks: community survey results and proposals," *Genetic Programming and Evolvable Machines*, vol. 14, pp. 3–29, 2013.
- [13] M. Schmidt and H. Lipson, "Distilling free-form natural laws from experimental data," *Science*, vol. 324, no. 5923, pp. 81–85, 2009.
- [14] Q. Chen, M. Zhang, and B. Xue, "Feature selection to improve generalization of genetic programming for high-dimensional symbolic regression," *IEEE Transactions on Evolutionary Computation*, vol. 21, no. 5, pp. 792–806, 2017.
- [15] W. La Cava, B. Burlacu, M. Virgolin, M. Kommenda, P. Orzechowski, F. O. de França, Y. Jin, and J. H. Moore, "Contemporary symbolic regression methods and their relative performance," *Advances in Neural Information Processing Systems*, vol. 2021, no. DB1, p. 1, 2021.
- [16] N. Makke and S. Chawla, "Interpretable scientific discovery with symbolic regression: a review," *Artificial Intelligence Review*, vol. 57, no. 1, p. 2, 2024.
- [17] B. Tran, B. Xue, and M. Zhang, "Genetic programming for feature construction and selection in classification on high-dimensional data," *Memetic Computing*, vol. 8, pp. 3–15, 2016.
- [18] P. G. Espejo, S. Ventura, and F. Herrera, "A survey on the application of genetic programming to classification," *IEEE Transactions on Systems, Man, and Cybernetics, Part C (Applications and Reviews)*, vol. 40, no. 2, pp. 121–144, 2009.
- [19] Y. Bi, B. Xue, and M. Zhang, *Genetic programming for image classification: An automated approach to feature learning*. Springer Nature, 2021, vol. 24.
- [20] G. S. Hornby, H. Lipson, and J. B. Pollack, "Generative representations for the automated design of modular physical robots," *IEEE Transactions on Robotics and Automation*, vol. 19, no. 4, pp. 703–719, 2003.
- [21] J. R. Koza, M. A. Keane, M. J. Streeter, W. Mydlowec, J. Yu, and G. Lanza, *Genetic programming IV: Routine human-competitive machine intelligence*. Springer Science & Business Media, 2005, vol. 5.
- [22] J. D. Lohn, G. S. Hornby, and D. S. Linden, "Human-competitive evolved antennas," *AI EDAM*, vol. 22, no. 3, pp. 235–247, 2008.
- [23] J. R. Koza, "Human-competitive results produced by genetic programming," *Genetic Programming and Evolvable Machines*, vol. 11, pp. 251–284, 2010.
- [24] S. Perkins and G. Hayes, "Evolving complex visual behaviours using genetic programming and shaping," in *Interdisciplinary Approaches to Robot Learning*. World Scientific, 2000, pp. 162–184.
- [25] D. C. Dracopoulos, D. Effraimidis, and B. D. Nichols, "Genetic programming as a solver to challenging reinforcement learning problems," *International Journal of Computer Research*, vol. 20, no. 3, p. 351, 2013.
- [26] D. Hein, S. Udluft, and T. A. Runkler, "Interpretable policies for reinforcement learning by genetic programming," *Engineering Applications of Artificial Intelligence*, vol. 76, pp. 158–169, 2018.
- [27] F.-A. Fortin, F.-M. De Rainville, M.-A. G. Gardner, M. Parizeau, and C. Gagné, "DEAP: evolutionary algorithms made easy," *J. Mach. Learn. Res.*, vol. 13, no. 1, p. 2171–2175, Jul. 2012.
- [28] T. Stephens, "gplearn: Genetic programming in Python, with a scikit-learn inspired API," <https://github.com/trevorstephens/gplearn>, 2015.
- [29] B. Burlacu, G. Kronberger, and M. Kommenda, "Operon C++: An efficient genetic programming framework for symbolic regression," in *Proceedings of the 2020 Genetic and Evolutionary Computation Conference Companion*, ser. GECCO '20. New York, NY, USA: Association for Computing Machinery, 2020, p. 1562–1570.
- [30] C. Huang, Y. Li, and X. Yao, "A survey of automatic parameter tuning methods for metaheuristics," *IEEE Transactions on Evolutionary Computation*, vol. 24, no. 2, pp. 201–216, 2020.
- [31] Z. Ma, H. Guo, Y.-J. Gong, J. Zhang, and K. C. Tan, "Toward automated algorithm design: A survey and practical guide to meta-black-box-optimization," *IEEE Transactions on Evolutionary Computation*, 2025, early access.
- [32] M. Chen, C. Feng, and R. Cheng, "MetaDE: Evolving differential evolution by differential evolution," *IEEE Transactions on Evolutionary Computation*, 2025, early access.
- [33] K. Staats, E. Pantridge, M. Cavaglia, I. Milovanov, and A. Aniyar, "TensorFlow enabled genetic programming," in *Proceedings of the Genetic and Evolutionary Computation Conference Companion*, ser. GECCO '17. New York, NY, USA: Association for Computing Machinery, 2017, p. 1872–1879.
- [34] F. Baeta, J. Correia, T. Martins, and P. Machado, "TensorGP – genetic programming engine in TensorFlow," in *Applications of Evolutionary Computation - 24th International Conference, EvoApplications 2021*. Springer, 2021.
- [35] R. Zhang, A. Lensen, and Y. Sun, "Speeding up genetic programming based symbolic regression using GPUs," in *Pacific Rim International Conference on Artificial Intelligence*. Springer, 2022, pp. 519–533.
- [36] Y. Tang, Y. Tian, and D. Ha, "EvoJAX: Hardware-accelerated neuroevolution," in *Proceedings of the Genetic and Evolutionary Computation Conference Companion*, ser. GECCO '22. New York, NY, USA: Association for Computing Machinery, 2022, p. 308–311.
- [37] R. T. Lange, "evosax: JAX-based evolution strategies," in *Proceedings of the Companion Conference on Genetic and Evolutionary Computation*, ser. GECCO '23. New York, NY, USA: Association for Computing Machinery, 2023, p. 659–662.
- [38] N. E. Toklu, T. Atkinson, V. Micka, P. Liskowski, and R. K. Srivastava, "EvoTorch: Scalable evolutionary computation in Python," 2023. [Online]. Available: <https://arxiv.org/abs/2302.12600>
- [39] B. Huang, R. Cheng, Z. Li, Y. Jin, and K. C. Tan, "EvoX: A Distributed GPU-accelerated Framework for Scalable Evolutionary Computation," *IEEE Transactions on Evolutionary Computation*, 2024, early access.
- [40] L. Wang, M. Zhao, E. Liu, K. Sun, and R. Cheng, "Tensorneat: A gpu-accelerated library for neuroevolution of augmenting topologies," *ACM Transactions on Evolutionary Learning and Optimization*, Apr. 2025.
- [41] Z. Liang, T. Jiang, K. Sun, and R. Cheng, "GPU-accelerated evolutionary multiobjective optimization using tensorized RVEA," in *Proceedings of the Genetic and Evolutionary Computation Conference*, ser. GECCO '24. New York, NY, USA: Association for Computing Machinery, 2024, p. 566–575.
- [42] Z. Liang, H. Li, N. Yu, K. Sun, and R. Cheng, "Bridging evolutionary multiobjective optimization and GPU acceleration via tensorization," *IEEE Transactions on Evolutionary Computation*, 2025, early access.
- [43] M. Abadi, A. Agarwal, P. Barham, E. Brevdo, Z. Chen, C. Citro, G. S. Corrado, A. Davis, J. Dean, M. Devin *et al.*, "TensorFlow: Large-scale machine learning on heterogeneous distributed systems," 2016. [Online]. Available: <https://arxiv.org/abs/1603.04467>
- [44] A. Paszke, S. Gross, S. Chintala, G. Chanan, E. Yang, Z. DeVito, Z. Lin, A. Desmaison, L. Antiga, and A. Lerer, "Automatic differentiation in PyTorch," in *NIPS-W*, 2017.
- [45] D. Guide, "CUDA C++ programming guide," *NVIDIA*, July, 2020.
- [46] G. Brockman, V. Cheung, L. Pettersson, J. Schneider, J. Schulman, J. Tang, and W. Zaremba, "OpenAI Gym," 2016. [Online]. Available: <https://arxiv.org/abs/1606.01540>

- [47] E. Todorov, T. Erez, and Y. Tassa, "MuJoCo: A physics engine for model-based control," in *2012 IEEE/RSJ International Conference on Intelligent Robots and Systems*. IEEE, 2012, pp. 5026–5033.
- [48] C. D. Freeman, E. Frey, A. Raichuk, S. Girgin, I. Mordatch, and O. Bachem, "Brax—a differentiable physics engine for large scale rigid body simulation," 2021. [Online]. Available: <https://arxiv.org/abs/2106.13281>
- [49] Genesis Authors, "Genesis: A generative and universal physics engine for robotics and beyond," December 2024. [Online]. Available: <https://github.com/Genesis-Embodied-AI/Genesis>
- [50] R. Poli, W. B. Langdon, and N. F. McPhee, *A Field Guide to Genetic Programming*. Lulu Enterprises, UK Ltd, 2008.
- [51] M. Pharr and R. Fernando, *GPU Gems 2: Programming techniques for high-performance graphics and general-purpose computation*. Addison-Wesley Professional, 2005.
- [52] M. Winter, M. Parger, D. Mlakar, and M. Steinberger, "Are dynamic memory managers on GPUs slow? a survey and benchmarks," in *Proceedings of the 26th ACM SIGPLAN Symposium on Principles and Practice of Parallel Programming*, 2021, pp. 219–233.
- [53] J. Nickolls, I. Buck, M. Garland, and K. Skadron, "Scalable parallel programming with CUDA," in *ACM SIGGRAPH 2008 Classes*, ser. SIGGRAPH '08. Association for Computing Machinery, 2008.
- [54] J. Sanders, *CUDA by Example: An Introduction to General-Purpose GPU Programming*. Addison-Wesley Professional, 2010.
- [55] E. Lindholm, J. Nickolls, S. Oberman, and J. Montrym, "NVIDIA Tesla: A unified graphics and computing architecture," *IEEE Micro*, vol. 28, no. 2, pp. 39–55, 2008.
- [56] M. Garland, S. Le Grand, J. Nickolls, J. Anderson, J. Hardwick, S. Morton, E. Phillips, Y. Zhang, and V. Volkov, "Parallel computing experiences with CUDA," *IEEE Micro*, vol. 28, no. 4, pp. 13–27, 2008.
- [57] T.-W. Huang, D.-L. Lin, C.-X. Lin, and Y. Lin, "Taskflow: A lightweight parallel and heterogeneous task graph computing system," *IEEE Transactions on Parallel and Distributed Systems*, vol. 33, no. 6, p. 1303–1320, Jun. 2022.
- [58] Y. Zhang and M. Zhang, "A multiple-output program tree structure in genetic programming," in *Proceedings of The Second Asian-Pacific Workshop on Genetic Programming*. Citeseer, 2004.
- [59] M. Cranmer, "Interpretable machine learning for science with PySR and symbolicregression. jl," 2023. [Online]. Available: <https://arxiv.org/abs/2305.01582>
- [60] D. Dua and C. Graff, "UCI machine learning repository," 2017. [Online]. Available: <http://archive.ics.uci.edu/ml>
- [61] F. Pedregosa, G. Varoquaux, A. Gramfort, V. Michel, B. Thirion, O. Grisel, M. Blondel, P. Prettenhofer, R. Weiss, V. Dubourg *et al.*, "Scikit-learn: Machine learning in Python," *the Journal of Machine Learning Research*, vol. 12, pp. 2825–2830, 2011.
- [62] S.-M. Udrescu and M. Tegmark, "AI Feynman: A physics-inspired method for symbolic regression," *Science Advances*, vol. 6, no. 16, p. eaay2631, 2020.
- [63] R. P. Ferreira, A. Martiniano, A. A. L. Ferreira, A. Ferreira, and R. J. Sassi, "Study on daily demand forecasting orders using artificial neural network," *IEEE Latin America Transactions*, vol. 14, pp. 1519–1525, 2016.
- [64] R. Quinlan, "Auto MPG," UCI Machine Learning Repository, 1993. [Online]. Available: <https://doi.org/10.24432/C5859H>
- [65] R. Kelley Pace and R. Barry, "Sparse spatial autoregressions," *Statistics & Probability Letters*, vol. 33, no. 3, pp. 291–297, 1997.
- [66] W. B. Langdon, "A many threaded CUDA interpreter for genetic programming," in *European Conference on Genetic Programming*. Springer, 2010, pp. 146–158.
- [67] S. Aeberhard, D. Coomans, and O. Y. de Vel, "Comparative analysis of statistical pattern recognition methods in high dimensional settings," *Pattern Recognit.*, vol. 27, pp. 1065–1077, 1994.
- [68] L. Rubini, P. Soundarapandian, and P. Eswaran, "Chronic Kidney Disease," UCI Machine Learning Repository, 2015, DOI: <https://doi.org/10.24432/C5G020>.
- [69] W. N. Street, W. H. Wolberg, and O. L. Mangasarian, "Nuclear feature extraction for breast tumor diagnosis," in *Electronic imaging*, 1993.
- [70] K. Nakai, "Yeast," UCI Machine Learning Repository, 1991. [Online]. Available: <https://doi.org/10.24432/C5KG68>

Enabling Population-Level Parallelism in Tree-Based Genetic Programming for GPU Acceleration (Supplementary Document)

S.I. PERFORMANCE COMPARISON WITH TENSORGP ON THE PAGIE POLYNOMIAL TASK

In the main body of this paper, we benchmarked EvoGP against several state-of-the-art symbolic regression libraries. During the preliminary evaluations, we also examined TensorGP [34], a library designed for GPU acceleration. However, its support for custom datasets was found to be limited, and the initial results indicated relatively lower performance. To maintain a consistent comparison with current state-of-the-art libraries, the results for TensorGP were therefore not included in the main body of the paper.

For completeness, we conducted an additional experiment on the Pagie polynomial task, which TensorGP supports natively. This experiment compared EvoGP, TensorGP, and other representative libraries (i.e., SRGPU, DEAP, and gplearn) under identical conditions to provide a direct performance assessment. The experimental environment and hyperparameter settings were consistent with those in Table II and Table III, and all GPU-based tests were performed on a single NVIDIA GeForce RTX 3090 GPU. The results, presented in Fig. S.1, indicate that TensorGP achieved lower throughput than other GPU-based libraries and also underperformed compared to CPU-based implementations.

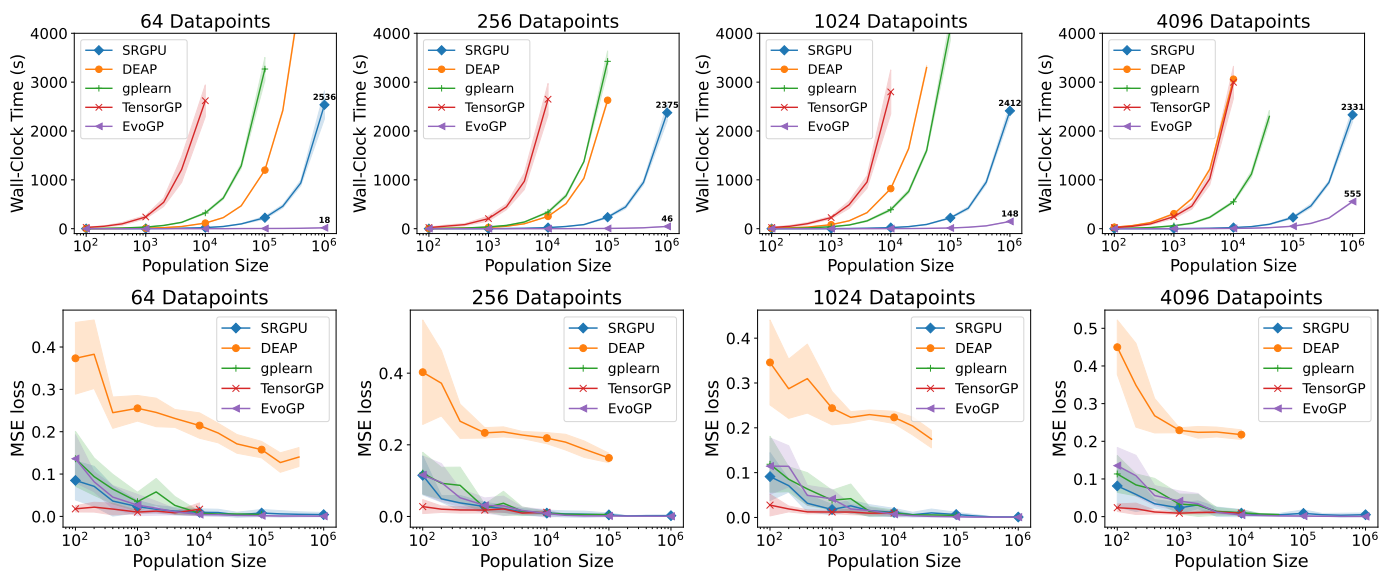


Fig. S.1: Comparison of EvoGP with TensorGP and other representative libraries on the Pagie polynomial benchmark. The top row shows total execution time as a function of population size, and the bottom row presents solution quality measured by MSE.

S.II. REPRODUCIBILITY AND SOFTWARE ENVIRONMENT

To facilitate the reproducibility of our experiments and provide comprehensive details regarding the computational environment, we present detailed versioning information for all symbolic regression libraries utilized in this study. Furthermore, we include specific build configurations for the *Operon* library to ensure transparency regarding compiler optimizations and backend selections.

A. Software Versions

Table S.I lists the specific versions or Git commit hashes for the Python packages and C++/CUDA libraries utilized in our benchmarks.

TABLE S.I
SOFTWARE LIBRARIES AND VERSIONING INFORMATION USED IN THE EXPERIMENTS.

Library	Type	Version / Commit Hash
DEAP	Python Package	v1.4.3
gplearn	Python Package	v0.4.2
PySR	Python Package	v1.5.9
EvoGP	Source Build	606f7f4aba8d1237cf0c818fe59c24457115b773
SRGPU	Source Build	e7f0eb80bc38c23df11a06244649a2453d0fae74
TensorGP	Source Build	f14708cb68238553cf8f735928837c2311264ab5
Operon	Source Build	d13d3ea826744c98287d0fd9df61f7af56d8d71a

B. Operon Build Details

The performance of *Operon* depends substantially on the underlying mathematical backend and compiler optimizations. Consequently, we provide the runtime version information and the precise CMake command used to build the library to ensure reproducibility.

1) *Runtime Version Information*: The output of the `./build/cli/operon_gp --version` command on our experimental platform is as follows:

Listing 1: Operon Version Output Details.

```
operon rev. d13d3ea Release Linux-6.12.35 x86_64, timestamp 2025-12-31T03:15:48Z
single-precision build using eigen 5.0.1, ceres n/a, taskflow 3.11.0
compiler: GNU 13.2.0, flags: -g -O3 -DNDEBUG -Wno-error
```

2) *CMake Build Command*: To enable the Eve math backend and thereby maximize performance on the target CPU hardware, we utilized the following CMake invocation:

Listing 2: CMake Command Used to Compile Operon with the Eve Backend.

```
cmake -S . \
-B build --preset build-linux \
-DCMAKE_BUILD_TYPE=Release \
-DMATH_BACKEND="Eve" \
-DBUILD_CLI_PROGRAMS=ON \
-DCMAKE_EXPORT_COMPILE_COMMANDS=ON \
-DCMAKE_CXX_FLAGS="-Wno-error" \
-DBUILD_TESTING=OFF \
-DBUILD_SHARED_LIBS=OFF \
-DCMAKE_POSITION_INDEPENDENT_CODE=ON \
-DCMAKE_TOOLCHAIN_FILE=/root/vcpkg/scripts/buildsystems/vcpkg.cmake \
-DVCPKG_OVERLAY_PORTS=./ports \
-DCMAKE_PREFIX_PATH=/root/vcpkg/installed/x64-linux \
-DCMAKE_C_COMPILER=/usr/bin/gcc \
-DCMAKE_CXX_COMPILER=/usr/bin/c++
```

S.III. GPOPS/S PERFORMANCE DATA FOR ALL LIBRARIES

TABLE S.II
DETAILED BREAKDOWN OF PYSR GPOPS/S PERFORMANCE ACROSS POPULATION AND DATASET SIZES

Population Size	60 Datapoints			392 Datapoints			20640 Datapoints			100000 Datapoints		
	Time	Avg. Size	GPops/s	Time	Avg. Size	GPops/s	Time	Avg. Size	GPops/s	Time	Avg. Size	GPops/s
100	127.94	333.71	1.68×10^6	423.20	381.91	3.56×10^6	3650.04	392.05	2.22×10^7	4164.54	463.53	1.11×10^8
500	603.14	288.50	1.36×10^6	2337.47	229.55	2.21×10^6	-	-	-	-	-	-
1,000	1150.52	334.77	1.87×10^6	-	-	-	-	-	-	-	-	-

TABLE S.III
DETAILED BREAKDOWN OF DEAP GPOPS/S PERFORMANCE ACROSS POPULATION AND DATASET SIZES

Population Size	60 Datapoints			392 Datapoints			20640 Datapoints			100000 Datapoints		
	Time	Avg. Size	GPops/s	Time	Avg. Size	GPops/s	Time	Avg. Size	GPops/s	Time	Avg. Size	GPops/s
100	3.10	9.15	1.78×10^6	11.01	9.02	3.22×10^6	521.42	9.90	3.90×10^6	2304.46	8.48	3.68×10^6
500	14.46	9.02	1.87×10^6	53.78	9.16	3.34×10^6	2439.16	9.24	3.91×10^6	-	-	-
1,000	29.03	9.36	1.94×10^6	109.25	9.34	3.35×10^6	4978.83	9.29	3.86×10^6	-	-	-
5,000	155.35	9.33	1.80×10^6	534.29	9.32	3.42×10^6	-	-	-	-	-	-
10,000	433.78	9.26	1.28×10^6	1659.54	9.36	2.22×10^6	-	-	-	-	-	-
50,000	2388.42	9.29	1.17×10^6	-	-	-	-	-	-	-	-	-

TABLE S.IV
DETAILED BREAKDOWN OF GPLEARN GPOPS/S PERFORMANCE ACROSS POPULATION AND DATASET SIZES

Population Size	60 Datapoints			392 Datapoints			20640 Datapoints			100000 Datapoints		
	Time	Avg. Size	GPops/s	Time	Avg. Size	GPops/s	Time	Avg. Size	GPops/s	Time	Avg. Size	GPops/s
100	7.95	421.27	2.16×10^7	7.73	213.04	9.63×10^7	11.62	16.69	2.46×10^8	26.56	4.14	1.58×10^8
500	65.16	1123.00	3.01×10^7	53.74	334.33	1.13×10^8	69.02	15.02	2.09×10^8	139.54	3.67	1.40×10^8
1,000	55.89	109.76	5.56×10^6	138.88	446.65	1.22×10^8	125.72	17.51	2.74×10^8	273.49	3.90	1.46×10^8
5,000	241.29	5.28	6.57×10^5	635.97	393.31	1.21×10^8	621.58	24.95	4.21×10^8	1203.28	3.97	1.66×10^8
10,000	486.40	5.27	6.50×10^5	1356.35	440.97	1.27×10^8	1558.67	27.55	3.75×10^8	2531.53	4.71	1.82×10^8
50,000	2502.93	5.25	6.30×10^5	-	-	-	-	-	-	-	-	-

TABLE S.V
DETAILED BREAKDOWN OF SRGPU GPOPS/S PERFORMANCE ACROSS POPULATION AND DATASET SIZES

Population Size	60 Datapoints			392 Datapoints			20640 Datapoints			100000 Datapoints		
	Time	Avg. Size	GPops/s	Time	Avg. Size	GPops/s	Time	Avg. Size	GPops/s	Time	Avg. Size	GPops/s
100	0.63	76.50	6.17×10^7	0.58	93.43	5.48×10^8	1.07	134.39	2.35×10^{10}	0.70	60.97	8.21×10^{10}
500	4.15	150.38	1.10×10^8	3.88	151.82	7.59×10^8	4.06	116.70	2.94×10^{10}	3.71	81.91	9.30×10^{10}
1,000	9.98	193.33	9.70×10^7	9.56	202.40	7.99×10^8	7.59	111.87	2.95×10^{10}	8.80	123.32	1.30×10^{11}
5,000	44.69	164.50	1.09×10^8	48.28	202.83	8.14×10^8	36.25	106.71	3.00×10^{10}	38.79	105.19	1.34×10^{11}
10,000	86.18	166.69	1.07×10^8	81.19	153.79	7.08×10^8	80.98	127.64	3.20×10^{10}	92.21	133.77	1.46×10^{11}
50,000	671.76	265.00	1.18×10^8	401.45	141.05	6.59×10^8	406.17	128.69	3.21×10^{10}	435.76	111.55	1.26×10^{11}
100,000	1247.69	249.99	1.19×10^8	851.06	167.16	7.35×10^8	784.60	128.64	3.35×10^{10}	1004.88	129.30	1.26×10^{11}
500,000	6079.53	218.63	1.07×10^8	5248.66	227.63	8.30×10^8	4088.10	116.60	2.93×10^{10}	4677.27	118.71	1.26×10^{11}

TABLE S.VI
DETAILED BREAKDOWN OF OPERON GPOPS/S PERFORMANCE ACROSS POPULATION AND DATASET SIZES

Population Size	60 Datapoints			392 Datapoints			20640 Datapoints			100000 Datapoints		
	Time	Avg. Size	GPOps/s	Time	Avg. Size	GPOps/s	Time	Avg. Size	GPOps/s	Time	Avg. Size	GPOps/s
100	0.08	402.12	2.84×10^9	0.19	400.63	8.45×10^9	4.19	376.45	1.88×10^{10}	6.71	336.03	5.20×10^{10}
500	0.32	473.41	4.49×10^9	0.83	482.12	1.19×10^{10}	13.81	430.74	4.29×10^{10}	45.00	434.43	5.69×10^{10}
1,000	0.55	454.55	4.98×10^9	1.44	460.11	1.35×10^{10}	55.20	474.11	2.07×10^{10}	116.24	454.86	4.23×10^{10}
5,000	2.78	479.52	5.21×10^9	8.71	487.41	1.12×10^{10}	292.27	486.24	2.07×10^{10}	575.76	465.43	4.63×10^{10}
10,000	6.66	486.38	4.41×10^9	17.83	483.29	1.07×10^{10}	547.45	468.78	1.85×10^{10}	910.28	480.79	5.38×10^{10}
50,000	33.61	475.78	4.27×10^9	98.74	482.26	9.65×10^9	3041.50	489.39	1.69×10^{10}	4960.14	463.82	4.84×10^{10}
100,000	77.99	474.46	3.66×10^9	223.00	488.90	8.65×10^9	7187.06	485.39	1.44×10^{10}	11626.46	458.33	4.17×10^{10}
500,000	892.91	467.66	1.79×10^9	2184.56	488.62	4.74×10^9	-	-	-	-	-	-
1,000,000	1098.94	464.58	2.54×10^9	2448.10	487.54	7.90×10^9	-	-	-	-	-	-

TABLE S.VII
DETAILED BREAKDOWN OF EVOGP GPOPS/S PERFORMANCE ACROSS POPULATION AND DATASET SIZES

Population Size	60 Datapoints			392 Datapoints			20640 Datapoints			100000 Datapoints		
	Time	Avg. Size	GPOps/s	Time	Avg. Size	GPOps/s	Time	Avg. Size	GPOps/s	Time	Avg. Size	GPOps/s
100	0.91	309.30	2.05×10^8	0.89	293.35	1.26×10^9	1.06	171.64	3.49×10^{10}	1.45	234.81	1.55×10^{11}
500	1.07	392.24	1.20×10^9	1.05	460.96	8.67×10^9	2.40	291.49	1.27×10^{11}	4.48	310.63	3.35×10^{11}
1,000	1.38	409.62	1.85×10^9	1.87	461.65	1.02×10^{10}	4.06	327.67	1.61×10^{11}	7.66	287.79	3.50×10^{11}
5,000	1.48	344.26	7.31×10^9	3.16	467.77	2.93×10^{10}	21.21	424.70	2.07×10^{11}	52.43	434.40	4.14×10^{11}
10,000	1.84	336.85	1.13×10^{10}	4.33	473.37	4.32×10^{10}	41.63	426.26	2.08×10^{11}	112.52	439.56	3.92×10^{11}
50,000	12.00	421.12	1.67×10^{10}	30.52	486.44	3.38×10^{10}	228.26	470.74	2.14×10^{11}	562.32	460.16	4.10×10^{11}
100,000	11.91	427.72	2.27×10^{10}	36.00	484.57	5.31×10^{10}	458.80	470.49	2.12×10^{11}	1155.62	467.02	4.05×10^{11}
500,000	34.62	374.19	3.25×10^{10}	163.11	487.93	5.87×10^{10}	2465.43	474.55	1.99×10^{11}	6188.84	466.23	3.78×10^{11}
1,000,000	74.96	409.84	3.29×10^{10}	327.49	490.13	5.87×10^{10}	5002.68	476.15	1.97×10^{11}	11668.21	454.52	3.90×10^{11}

S.IV. PERFORMANCE SUMMARY FOR THE FIXED GENERATION

TABLE S.VIII
PERFORMANCE AND COMPUTATIONAL TIME ACROSS TASKS AND POPULATION SIZES.

Task Type	Generations	Task Identifier	Pop Size	Performance	Wall-clock Time (s)
Symbolic Regression	900	Daily Demand Forecasting	200	377.004 ± 734.034	1.890 ± 0.067
			1000	12.809 ± 10.681	3.928 ± 0.104
			5000	1.400 ± 3.311	7.383 ± 0.463
		Auto MPG	200	11.025 ± 3.517	2.209 ± 0.047
			1000	8.130 ± 2.515	5.771 ± 0.174
			5000	5.031 ± 0.812	16.725 ± 0.315
		California Housing	200	0.535 ± 0.060	13.736 ± 0.978
			1000	0.408 ± 0.085	47.688 ± 9.969
			5000	0.354 ± 0.054	224.483 ± 7.479
		Feynman I.9.18	200	2.253e-3 ± 1.727e-3	24.540 ± 2.785
			1000	6.961e-4 ± 7.430e-4	98.195 ± 7.242
			5000	2.783e-4 ± 2.816e-4	473.305 ± 18.692
Classification	300	Wine	200	0.843 ± 0.109	60.061 ± 1.297
			1000	0.956 ± 0.013	70.997 ± 1.276
			5000	0.981 ± 0.008	98.401 ± 7.476
		Chronic Kidney Disease	200	0.943 ± 0.013	60.336 ± 1.961
			1000	0.963 ± 0.015	68.899 ± 3.310
			5000	0.973 ± 0.010	105.580 ± 5.803
		Breast Cancer Wisconsin	200	0.960 ± 0.009	63.457 ± 3.817
			1000	0.973 ± 0.005	69.717 ± 0.014
			5000	0.978 ± 0.005	122.362 ± 5.190
		Yeast	200	0.507 ± 0.026	62.417 ± 1.732
			1000	0.553 ± 0.033	81.128 ± 6.065
			5000	0.596 ± 0.010	214.529 ± 13.796
Robotics Control	100	Swimmer	200	369.509 ± 1.414	791.546 ± 99.421
			1000	373.577 ± 2.363	891.185 ± 65.661
			5000	376.662 ± 2.585	735.877 ± 57.907
		Hopper	200	1399.618 ± 448.981	354.702 ± 25.832
			1000	2444.291 ± 464.516	386.617 ± 21.714
			5000	2748.185 ± 505.279	503.509 ± 2.800
		Walker2d	200	1550.955 ± 334.275	324.897 ± 62.063
			1000	1905.647 ± 189.443	553.908 ± 19.456
			5000	2550.197 ± 385.302	1233.198 ± 9.948
		Halfcheetah	200	5545.219 ± 716.671	1175.703 ± 77.945
			1000	11313.934 ± 3181.319	1458.846 ± 7.558
			5000	14114.018 ± 3136.102	3701.693 ± 22.334

* The best performances are highlighted in bold.

* Performance metrics: (1) Symbolic Regression: MSE (lower is better); (2) Classification: Accuracy (higher is better); (3) Robotics Control: Cumulative Reward (higher is better).